Resource

Cell Reports

Kinetics and Mechanism of Mammalian Mitochondrial Ribosome Assembly

Graphical Abstract

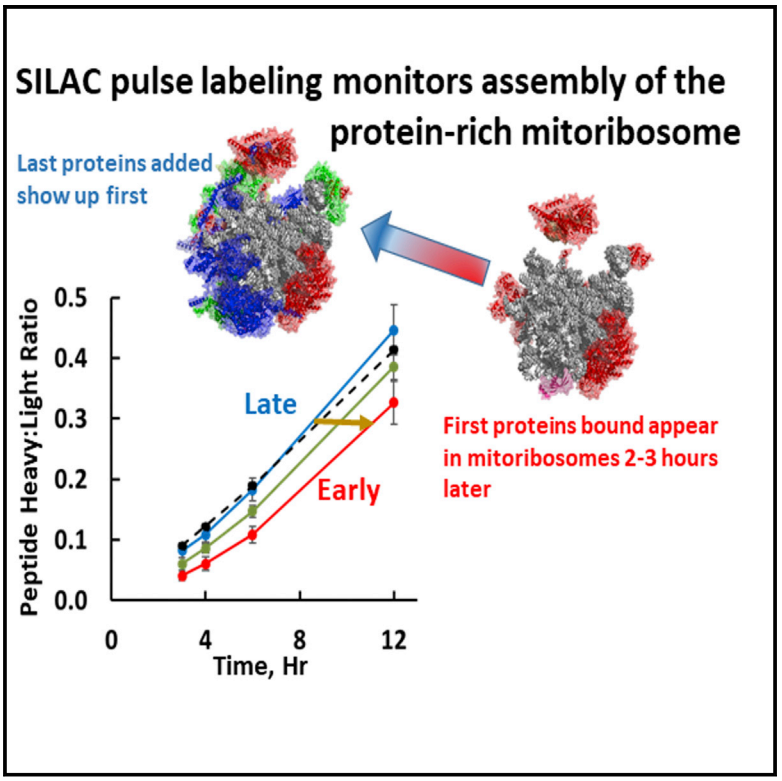

Highlights

- Pulse-chase SILAC provides a coarse-grained model for mitoribosome assembly
- Assembly of the protein-rich mitoribosome requires 2–3 hr
- Most mitoribosomal proteins are synthesized in excess and degraded if not assembled
- Mitoribosomal proteins implicated in human disease bind early during assembly

Authors

Daniel F. Bogenhagen, Anne G. Ostermeyer-Fay, John D. Haley, Miguel Garcia-Diaz

Correspondence

daniel.bogenhagen@stonybrook.edu

In Brief

Recent cryo-EM studies provided detailed structures of the protein-rich mammalian mitoribosome, but the process of their assembly is poorly understood. Bogenhagen et al. use SILAC pulse labeling to determine the order of addition of mitoribosomal proteins (MRPs) to provide a structure-based kinetic model for assembly of mammalian mitoribosomes.

Bogenhagen et al., 2018, Cell Reports *22*, 1935–1944
February 13, 2018
https://doi.org/10.1016/j.celrep.2018.01.066

CellPress

Cell Reports
Resource

Kinetics and Mechanism of Mammalian Mitochondrial Ribosome Assembly

Daniel F. Bogenhagen,[1,4,*] Anne G. Ostermeyer-Fay,[1] John D. Haley,[2,3] and Miguel Garcia-Diaz[1]
[1]Department of Pharmacological Sciences
[2]Department of Pathology
[3]Proteomics Center
Stony Brook University, Stony Brook, NY 11794-8651, USA
[4]Lead Contact
*Correspondence: daniel.bogenhagen@stonybrook.edu
https://doi.org/10.1016/j.celrep.2018.01.066

SUMMARY

Mammalian mtDNA encodes only 13 proteins, all essential components of respiratory complexes, synthesized by mitochondrial ribosomes. Mitoribosomes contain greatly truncated RNAs transcribed from mtDNA, including a structural tRNA in place of 5S RNA as a scaffold for binding 82 nucleus-encoded proteins, mitoribosomal proteins (MRPs). Cryoelectron microscopy (cryo-EM) studies have determined the structure of the mitoribosome, but its mechanism of assembly is unknown. Our SILAC pulse-labeling experiments determine the rates of mitochondrial import of MRPs and their assembly into intact mitoribosomes, providing a basis for distinguishing MRPs that bind at early and late stages in mitoribosome assembly to generate a working model for mitoribosome assembly. Mitoribosome assembly is a slow process initiated at the mtDNA nucleoid driven by excess synthesis of individual MRPs. MRPs that are tightly associated in the structure frequently join the complex in a coordinated manner. Clinically significant MRP mutations reported to date affect proteins that bind early on during assembly.

INTRODUCTION

Normal cell physiology relies on a close interaction between the nuclear and mitochondrial genomes to support oxidative metabolism. Biogenesis of the mitochondrial respiratory chain depends on coordinated expression of 13 proteins encoded in mtDNA with nearly 70 proteins that are nuclear gene products. The synthesis of this small number of mtDNA-encoded proteins occurs on mitochondrial ribosomes that are entirely distinct from cytoplasmic ribosomes. The mtDNA genome contributes only the RNA components of mitoribosomes. The rRNA genes are expressed by a single subunit mtRNA polymerase, POLRMT, along with mRNAs and tRNAs in long polycistronic precursors. In higher eukaryotes, although not in yeast, the rRNAs are co-localized with genes for $tRNA^F$ and $tRNA^V$ in a relatively long-lived precursor termed RNA 4 (Gelfand and Attardi, 1981). The biogenesis of mitoribosomes depends on coordinated synthesis of 82 mitochondrial ribosomal proteins (MRPs) encoded in nuclear DNA, which must be translated on cytoplasmic ribosomes and individually imported into mitochondria. It is apparent that building a mitoribosome is a difficult logistical task comparable to the complexity of assembling the entire respiratory chain.

The structures of mitoribosomes have been elucidated at near atomic resolution by two groups employing recent advances in cryoelectron microscopy (cryo-EM) methods (Amunts et al., 2015; Greber et al., 2015). Some of the unique features of the mitoribosomes are as follows: (1) As inferred from the human mtDNA sequence (Anderson et al., 1981), the rRNAs of large and small subunits of the mammalian ribosome were reduced in size during evolution to ~60% of the size of the corresponding *E. coli* rRNAs, with numerous deletions that shorten or eliminate secondary structure elements. (2) The 5S rRNA found in the central protuberance of the large subunit of nearly all standard prokaryotic and eukaryotic cytoplasmic ribosomes is absent from mammalian mitoribosomes, where it has been replaced by tRNA (generally $tRNA^V$ or $tRNA^F$, which are adjacent to the 12S rRNA gene in mtDNA). (3) Several protein subunits conserved in other ribosomes are absent from mitoribosomes, often reflecting corresponding deletions of their rRNA binding sites. (4) Despite truncation of the rRNA component, the overall mass is essentially conserved, as mitoribosomes contain a significant number of novel mitochondrial-specific polypeptides whose locations were only elucidated when the cryo-EM structures were resolved. (5) The tight organization of mitochondrial rRNA genes completely lacks intergenic spacer regions found in other rRNA gene regions, requiring precise incisions by RNases P and ELAC2 for rRNA maturation. (6) *S. cerevisiae* has followed a different evolutionary path to adopt unlinked rRNAs even larger than those found in *E. coli*, along with a distinct pattern of altered ribosomal proteins (Amunts et al., 2014; Desai et al., 2017). Thus, this organism is not a suitable model for studies of mammalian mitoribosome structure or function, although it bears its own intrinsic interest.

Despite the exciting advances in understanding the structure of mitoribosomes, we have few insights into the assembly of these macromolecular machines. In contrast, decades of research exploring the mechanism of bacterial ribosome assembly have provided robust models for assembly of both the large and small subunits (Shajani et al., 2011). This wealth of information is not readily applicable to mitoribosomes due to extensive structural changes during evolution as noted above.

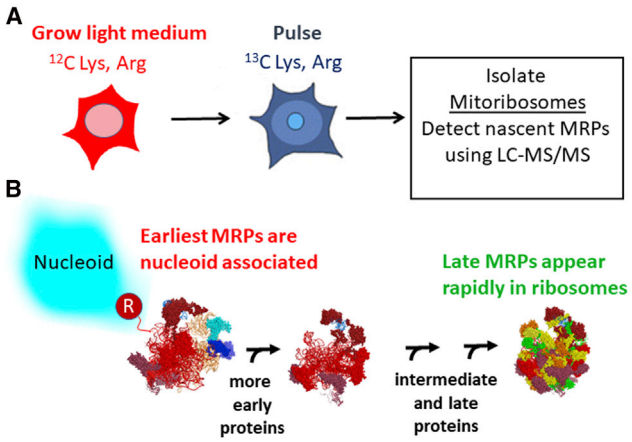

Figure 1. SILAC Labeling Resolves Steps in Mitoribosome Assembly

(A) The SILAC pulse-labeling approach.

(B) Newly synthesized rRNA is shown as a hypothetical folded structure emanating from mtRNA polymerase (R) with 12S rRNA (orange) still linked to $tRNA^V$ and 16S rRNA (red) as in the RNA 4 precursor. The actual conformation of the nascent RNA is unknown. MRP polypeptides begin to bind nascent rRNA at the nucleoid (Bogenhagen et al., 2014) and assembly intermediates progress to complete mitoribosomes after some delay. In contrast, late-binding proteins are less likely to be found in nucleoid preparations and appear more rapidly in fully assembled, mature mitoribosomes at rates distinguishable by SILAC pulse labeling.

Coordinating assembly of a mitoribosome is clearly a daunting task, since it requires import of as many structural proteins as the entire respiratory chain. We know that the assembly of a simpler structure, NADH dehydrogenase, requires nearly 24 hr for the 44 component proteins to join the complex (Guerrero-Castillo et al., 2017; Ugalde et al., 2004). The kinetics of mitoribosome assembly may be limited by the time required to import the 82 individual MRPs into mitochondria. It is evident that novel approaches are required to study mitoribosome assembly.

In this paper, we report proteomic experiments to study the kinetics of accumulation of nascent MRPs in mitochondria and their general order of addition during mitoribosome assembly. These experiments employed pulse labeling with stable isotopes (SILAC) to track the appearance of newly synthesized MRPs in isolated mitochondria and in mature mitoribosomes. SILAC permits detection of the newly synthesized polypeptides that incorporated ^{13}C-labeled lysine and arginine using mass spectrometry. We previously reported that a subset of newly synthesized MRPs is selectively associated with mtRNA at the mtDNA nucleoid, suggesting that these MRPs represent some of the first proteins to bind nascent rRNA (Figure 1; Bogenhagen et al., 2014). The current study tests the hypothesis that SILAC labeling can be used to dissect later steps in mitoribosome assembly. We found that MRPs are synthesized and imported into mitochondria at rates greater than required for mitoribosome assembly and are either built into mitoribosomes or, if they cannot be assembled, degraded. Some MRPs appear in mature ribosomes much more rapidly than others. We reasoned that the first MRPs to appear in mature mitoribosomes would be the last polypeptides added to complete assembly (Figure 1). In contrast, the first MRPs bound to nascent rRNA only appear in mature mitoribosomes after a delay. The data revealed several examples of pairs or small groups of MRPs that share extensive protein-protein interactions and join the mitoribosome with similar kinetics in a coordinated manner. Therefore, we analyzed the interactions between MRPs in the mitoribosome structure. The combination of SILAC pulse-labeling results and structural analysis provides a working model for the kinetic mechanism of mitoribosome assembly interpretable in light of the cryo-EM structure of the mitoribosome.

RESULTS

Kinetic Analysis of Mitoribosome Assembly

We conducted a series of SILAC experiments in which HeLa cells were pulse labeled with $^{13}C_6$ lysine and arginine (K6R6) for various time intervals (Experimental Procedures) to track the kinetic appearance of newly synthesized MRPs containing a high content of $^{13}C_6$ in completed mitoribosomes, indicated by a high ratio of "heavy" to "light" peptides, or a high H:L ratio. This ratio is analogous to a specific activity measurement in a radioactive labeling study. A broad survey of protein turnover rates included data suggesting that MRPs labeled during long-term SILAC are generally stable through the time course of our experiments (Schwanhäusser et al., 2011), so that the content of unlabeled MRPs, the denominator in the H:L ratio calculation, is not changed significantly over this interval. In growing cells, we would expect that labeling for a period of time equal to one cell generation time would result in 50% "heavy" MRPs. Similarly, simple exponential growth kinetics (using $N(t) = N_o\, e^{ln2t/Tg}$) predict that a 4-hr labeling should result in 12% "heavy" MRPs if the generation time (Tg) is 24 hr. A more complete description of the predicted labeling kinetics is provided in Supplemental Experimental Procedures. The SILAC approach tests the hypothesis that mitoribosome assembly is a rapid process, in which case all MRPs in fully assembled mitoribosomes would be labeled to a comparable extent. Mitoribosome purification followed the classical method developed by the O'Brien lab (Matthews et al., 1982) using two successive sucrose gradient separations under high-salt conditions as adapted in recent cryo-EM studies of the mitoribosome (Amunts et al., 2015; Greber et al., 2015). Gradient fractions containing intact 55S, 39S, and 28S mitoribosomes were identified by immunoblotting with antibodies to individual subunits (usually uL10m or uL13m and uS15m or uS17m; Figure S1). Proteins were recovered and submitted for digestion and mass spectrometry. To examine early kinetics of assembly, we used shorter labeling times of 3, 4, 6, or 12 hr. The results of triplicate experiments (Table S1) show that individual MRPs exhibit distinct kinetics of accumulation in mature mitoribosomes, with H:L ratios varying by over 2-fold at early labeling intervals. Figures 2A and 2B show the H:L ratios of individual MRPs after 3- and 4-hr labeling intervals for large subunit (LSU) and small subunit (SSU) proteins, respectively, indicating that proteins behaved consistently at a variety of pulse times. Higher values for the ribosome H:L ratio after short labeling intervals reflect more rapid appearance of newly synthesized protein in mature mitoribosomes (blue in Figure 2), while others appear more slowly (red) or at intermediate rates (green). Figures 2C and 2D illustrate the average kinetic patterns observed for the

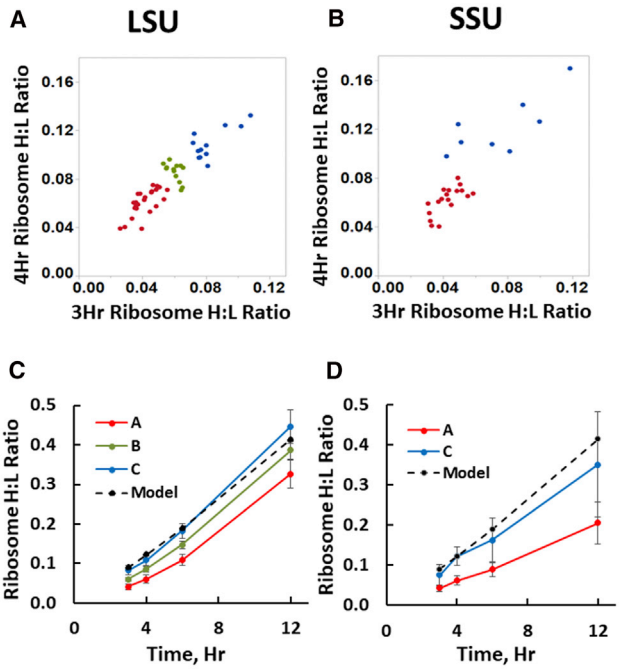

Figure 2. MRPs Appear in Mitoribosomes at Different Rates

(A and B) Scatterplots of H:L ratios observed for individual LSU (A) and SSU (B) MRPs after 3 and 4 hours of SILAC labeling. Points representing MRPs that have consistently low H:L ratios (Table S1) are designated class A (red), while those that appear more rapidly in mitoribosomes are class C (blue). For the larger set of LSU polypeptides, an intermediate class B is also designated (green).

(C and D) Average H:L ratios (± SD) for the early, intermediate and late classes of MRPs for the LSU (C) and SSU (D), as identified in Table S1. The dashed line shows the H:L ratios expected for the rate of mitoribosome synthesis required to sustain a constant cellular complement of mitoribosomes in growing cells (see Supplemental Experimental Procedures). Some MRPs were not included in this analysis because of insufficient numbers of peptides or, for bL33m, atypically rapid accumulation (discussed in the text). See also Figures S1 and S2.

rapidly appearing class C MRPs (blue) in contrast to more slowly incorporated class A MRPs (red) for the LSU and SSU, respectively. The class C MRPs appear in completed mitoribosomes at a rate comparable to that predicted by a mathematical model (Supplemental Methods) shown by the dashed line in Figure 2 that assumes preexisting mitoribosomes are relatively stable and new MRPs are synthesized to maintain a steady cellular content of mitoribosomes in growing cells.

We consider three alternative hypotheses to account for the varied rates of accumulation of MRPs in mitoribosomes. First, the logic in Figure 1 suggests that the class A MRPs may accumulate more slowly if they are incorporated into assembly intermediates that require more time to appear in intact mitoribosomes. An alternative hypothesis is that some nascent MRPs may be incorporated more rapidly by exchanging into preexisting mitoribosomes. A third consideration is that some nascent MRPs imported into mitochondria may be effectively diluted by larger pools of preexisting unlabeled MRPs, which could delay their appearance in intact mitoribosomes.

The hypothesis that the kinetics in Figure 2 could be explained by rapid exchange of MRPs into preexisting mitoribosomes is addressed by considering the behavior of one protein, bL33m, which accumulates at a rate far faster than any other MRP (Table S1), and which was omitted from the analysis for this reason. Figures S2A and S2B show that the mitoribosomal H:L ratio of bL33m was 0.21 after only 3 hr of labeling, increasing to 1.11 in a 12-hr labeling, which requires replacement of over half the copies of bL33m within 12 hr. Other rapidly appearing class C MRPs accumulated at a rate not appreciably greater than predicted by the mathematical model shown with the dashed lines in Figures 2C and 2D. No other MRP showed similar labeling kinetics. The exceptional assembly kinetics of bL33m suggest that exchange of newly synthesized MRPs into preexisting mitoribosomes is not a major factor for all other MRPs.

The second alternative hypothesis to explain differential assembly kinetics in Figure 2 is that the isotopically labeled MRPs that assemble more slowly may be diluted by larger pools of preexisting free, unlabeled polypeptides. We addressed this in two ways. First, we note that neither the rapidly appearing uS15m nor the slowly appearing uL10m featured a large pool of free protein in Figure S1. We surveyed six other class A MRPs for the presence or absence of large pools of free precursor proteins using immunoblotting of sucrose gradient fractions (Figure S2C), revealing several with small pools of free protein (uS17m, bL19m, and mL44) and others with larger pools (mL45, mS23, and mS27). This showed no correlation between assembly class and the relative size of precursor pools. In addition, we performed a separate analysis of the relative synthesis rates, assembly rates, and stability of MRPs below. The results of these analyses are consistent with the hypothesis that the class A MRPs bind early on during ribosome assembly while the class C MRPs appear first in intact mitoribosomes, because they represent the last MRPs to bind to complete the assembly of stable 39S and 28S subunits.

Nascent Early-Binding MRPs Complete Their Assembly into Mature Mitoribosomes during a Chase Interval

We performed additional pulse-chase labeling experiments to test whether the early binding proteins would ultimately appear in intact mitoribosomes along with the late-binding proteins. HeLa cells pulse labeled with K6R6 for 4 hr were incubated for an additional 10-hr "chase" with normal ^{12}C-labeled lysine and arginine. Figures 3A and 3B show comparisons of the labeling intensity for individual 39S and 28S MRPs after the pulse and pulse-chase incubations. The early-binding (class A) MRPs identified in Table S1 and Figure 2 (red in Figure 3) tend to reside in the lower regions of these plots, since their low H:L ratios after the pulse increase during the chase, as expected if labeled copies of these MRPs initially associated within incomplete assembly intermediates during the pulse. Distinct behavior of early and late MRPs can also be expressed by the ratio of H:L values with and without the chase, the P4C10/P4 ratio (Figures 3C and 3D). Clearly, the putative early-binding proteins increase significantly in H:L ratio during the chase as the intermediates in which they bind initially complete assembly. In contrast, the late-binding MRPs (blue) tend to reside in the upper region of the plots in Figures 3A and 3B, and the average H:L ratio for this group

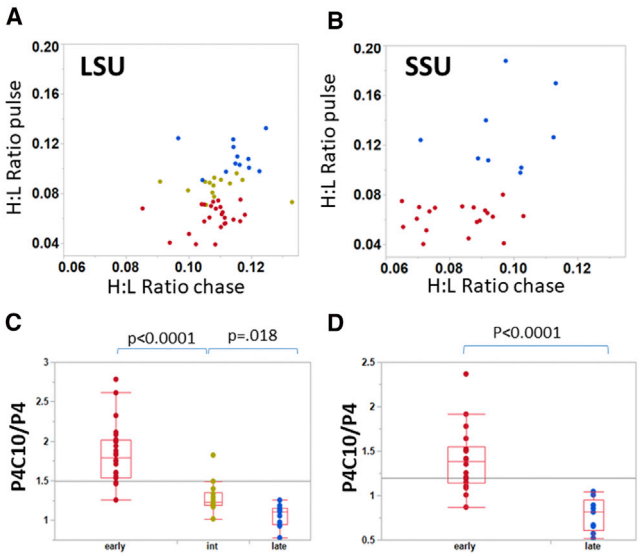

Figure 3. Mitoribosome Assembly Intermediates Containing Early-Binding Proteins Complete Assembly during Chase Incubation

(A and B) Scatterplots of the H:L ratios of individual LSU (A) and SSU (B) polypeptides, after the 4-hr pulse (ordinate) or after an additional 10-hr chase incubation (abscissa). Early- and late-binding proteins identified in Figure 2 are in red and blue, respectively, with intermediate LSU proteins in gold-green.

(C and D) The early, intermediate, and late classes of assembled MRPs in the LSU (C) and SSU (D) show statistically significant differences in P4C10/P4, the ratio of H:L values after and before the chase. Here and in Figure 4E, the horizontal lines indicate the mean value for all data points. See also Table S1.

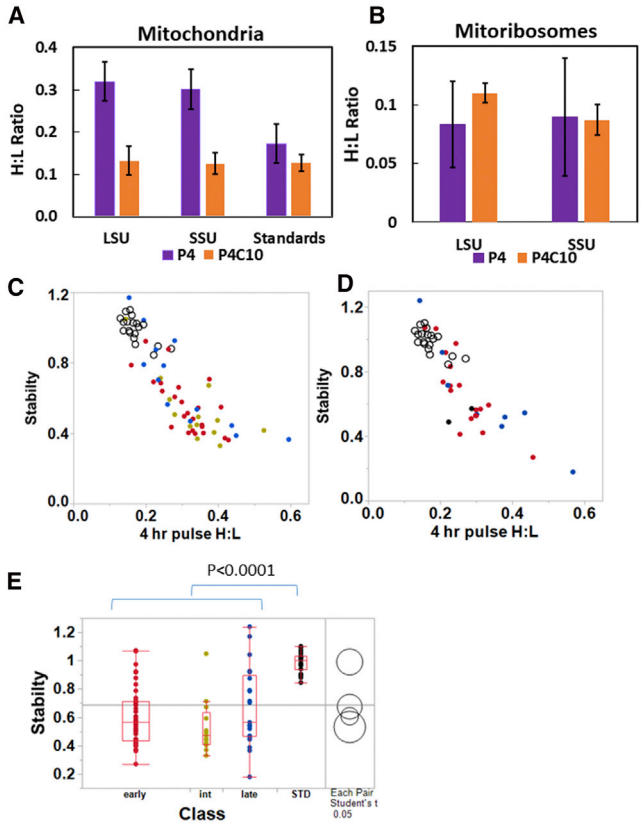

Figure 4. MRPs Are Synthesized and Imported in Excess and Can Be Unstable if Not Assembled

(A) The H:L ratio immediately after 4 hr of pulse labeling is greater for MRPs than for a standard set of mitochondrial proteins, indicating a higher rate of synthesis and mitochondrial import, but the H:L ratio of MRPs declines during a 10-hr chase to a value not significantly different from the stable standard proteins. Mean values are shown ± SD.

(B) The H:L values observed for MRPs in assembled mitoribosomes before and after the chase are shown for comparison. The large SE after the pulse reflects variable assembly kinetics of individual proteins and is significantly smaller after the chase. Note the change in scale of the ordinate compared to (A).

(C and D) The stability of LSU (C) and SSU (D) MRPs in early (red), intermediate (green), and late (blue) assembly classes is plotted against the H:L ratio after the pulse. Standard proteins are shown with open circles in both plots.

(E) The stabilities (P4C10/expected) of early, intermediate, and late assembly classes of MRPs are significantly lower than those of the standard proteins, but not significantly different from one another.

See also Tables S1 and S2.

actually decreases slightly during the chase (Figures 3C and 3D), revealing a statistically significant difference from the early-binding proteins ($p < 0.0001$). The late-binding proteins were incorporated quickly into mitoribosomes during the pulse. The continuous synthesis and assembly of unlabeled protein during the chase led to a slight decline in their H:L ratios.

MRPs Are Synthesized and Imported in Excess and Can Be Unstable if Not Assembled

Our results support the model that the distinct kinetics of incorporation of different MRPs into mitoribosomes principally reflects their relative assembly order. To further test the possibility that differences in the ability of individual nascent MRPs to exchange with the pool of free polypeptides or their general stability might influence the apparent assembly kinetics, we also monitored the rates of synthesis and mitochondrial import and the stability of MRPs by determining the H:L ratio of the total mitochondrial pool of each protein in pulse-chase SILAC experiments. In parallel with our mitoribosome pulse-chase experiment, samples of total mitochondrial protein obtained after 4-hr pulse labeling with and without a 10-hr chase (P4C10 and P4, respectively) were analyzed by liquid chromatography-tandem mass spectrometry (LC-MS/MS) to determine H:L ratios of the combined population of free and mitoribosome-bound copies of each MRP. Table S2 shows the results obtained for MRPs and for a set of standard proteins identified in Table S2 and summarized in the histogram in Figure 4A. The standard proteins declined from an initial average H:L value of 0.172 to 0.127 during the chase. This decrease is explained by the continued growth of the cells in ^{12}C medium during the chase, which we expect to dilute labeled proteins and to reduce the H:L value by 25%. Clearly, the rates of synthesis and importation of these standard proteins are commensurate with the cell growth rate, and there is negligible wastage of newly made protein. In contrast, the MRPs are synthesized and imported at high rates, with H:L ratios averaging ~0.3. Many copies of these nascent MRPs are degraded in the 10-hr chase as the H:L ratio declines to statistically the same level as the standard proteins (Figure 4A). The magnitude of this decline cannot be explained by dilution with other newly synthesized protein but must reflect

degradation. The final H:L ratio of the total mitochondrial pool of MRPs is very close to that in intact mitoribosomes (Figure 4B). Thus, the degradation process mostly operates on free copies of MRPs in this time frame.

We next sought to determine whether the putative early and late MRPs exhibited differences in stability. This is an important issue, since it may be argued that the rapid appearance in intact mitoribosomes of the MRPs we designate as late might be due to their exchange with polypeptides within preexisting mitoribosomes. To express the behavior of proteins concisely, we defined a stability parameter as the ratio of the observed H:L value after the 10-hr chase to that expected due to the dilution of labeled protein during the chase. A very long-lived protein would be expected to have a stability parameter of 1.0. In keeping with this, the 19 standard proteins had an average stability (± SD) of 0.99 ± 0.07. Figures 4C and 4D show that most of the early and late LSU and SSU MRPs, respectively, are much less stable than the standard proteins shown as open circles. Statistical analysis using pairwise t tests showed that all three classes of early, intermediate, and late MRPs were significantly less stable than the standard proteins ($p < 0.0001$), but there was no significant difference in stability among these three classes of MRPs (Figure 4E). Similar results were obtained in other experiments with 3-hr pulse labeling followed by an 8-hr chase (data not shown). While further experiments will be required to explore the degradation rates of nascent MRPs in greater detail, we found no evidence that protein stability or exchange into preexisting mitoribosomes plays a major role in the different assembly kinetics of early and late MRPs, except for the counter-example of bL33m noted above. This does not rule out the possibility that there may be some slower exchange of other proteins.

Developing a Kinetic Model for Mitoribosome Assembly

The foregoing results distinguish broad classes of early- and late-binding MRPs. The positions these proteins occupy in the final model of the mitoribosome are important to understand the process of mitoribosome assembly. The mammalian mitoribosome has a much higher protein/RNA content and smaller rRNA scaffolds than the bacterial ribosome, so that protein-protein interactions are likely to be more important in mitoribosome assembly. Table S3 shows the rosters of early-, intermediate-, and late-binding MRPs in the SSU and LSU. The assembly order is not solely determined by the extent of a protein's interaction with rRNA (Figure S3). We noted many instances in which proteins with similar assembly kinetics shared extensive binding interfaces, raising the possibility that adjacent proteins might assemble in a coordinated manner. The binding affinity of a protein-protein interaction in a crystal structure is generally related to the buried surface area (BSA) (Kastritis and Bonvin, 2012), except in cases where conformational changes take place upon binding, which is likely at least for some proteins in the context of ribosome assembly. We conducted a comprehensive analysis of the size of protein-protein interaction surfaces for the model of the human mitoribosome (PDB: 3J9M) determined using the PDBePISA site (www.ebi.ac.uk/pdbe/pisa/). BSA calculations have been used previously in the analysis of mitoribosome cryo-EM structures (Brown et al., 2014). BSA values larger than 600–850 $Å^2$ are considered to indicate a biologically significant interface (Krissinel, 2010). We estimated that BSA >1,000 $Å^2$ would likely result in strong interactions that would influence the assembly pathway. The exact value set as a threshold for strong interactions is somewhat arbitrary, but we selected this value because most homodimers have a BSA >1,000 $Å^2$ (Bahadur et al., 2003). The BSAs for pairs of MRPs are shown in Figure S4, where proteins are ordered as in Table S3. It is apparent that small sets of proteins with similar assembly kinetics can often be grouped into modules that share extensive interactions. Indeed, this principle guided the subdivision of proteins within groups shown in Table S3 and Figure S4. Our goal was not to determine a unique sequence of binding events, since it is well accepted even for the simpler bacterial ribosome that assembly is best described as a general landscape that may proceed through a variety of detailed pathways (Talkington et al., 2005). Instead, the model indicates where early- and late-binding proteins reside in the mature mitoribosome structure with a full realization that large-scale structural remodeling is likely to occur at each stage of assembly. This model provides a frame of reference for further studies to refine the assembly process. The model is limited by the fact that mL52, bL36m, bS18m, and mS37 did not produce a sufficient number of peptides for our mass spectrometry (MS) analysis and that uL1m and bL12m are not present in the structural model we used, 3J9M.

SSU Assembly

Models for bacterial ribosome assembly cannot be applied directly to the mitoribosome, since a number of critical early-binding or primary proteins of the bacterial ribosome such as bS20, bS4, and bS8 were lost during evolution. Table S3 identifies the set of early-binding 28S proteins, most of which reside in two relatively large groups at the head and lower body/foot of the elongated 12S RNA core (Figure 5A). Figure 5 illustrates early- and late-binding MRPs as red and blue, respectively. Individual MRPs within binding clusters are illustrated in Figure S5. In one cluster, bS16m, mS22, and mS40 interact in the lower body in a complex that makes RNA contacts almost exclusively with the 5′ domain of 12S rRNA (Figures 5, S3, and S5B). The fact that this set of proteins interacts with the first 12S rRNA sequences available as transcription proceeds is consistent with the hypothesis that the organization of this domain may seed the entire assembly process shown in Figure 5C. Interestingly, one member of this set, mS22, does not contact 12S rRNA directly but joins at an early stage through its interactions with bS16m and mS40. This module extends to the foot with mS34 and mS27 interacting with the 3′ domain of 12S rRNA. Binding of this subgroup is followed closely by that of uS5m, likely due to the tight interaction of this protein with uS22m and mS40. uS5m is differentially colored in Figure 5 to illustrate how it bridges the two major groups of early proteins. The second set of early SSU proteins binding to the major 3′ domain of 12S rRNA in the head region includes three closely interacting proteins with extensive RNA contacts (uS7m, uS9m, and mS29) as well as three other proteins (mS31, mS35, and mS39) that substantially lack RNA interactions (Figure S3) and appear to be recruited by the other group members. A smaller set of early proteins in Table S3 includes mS23, which shares a binding

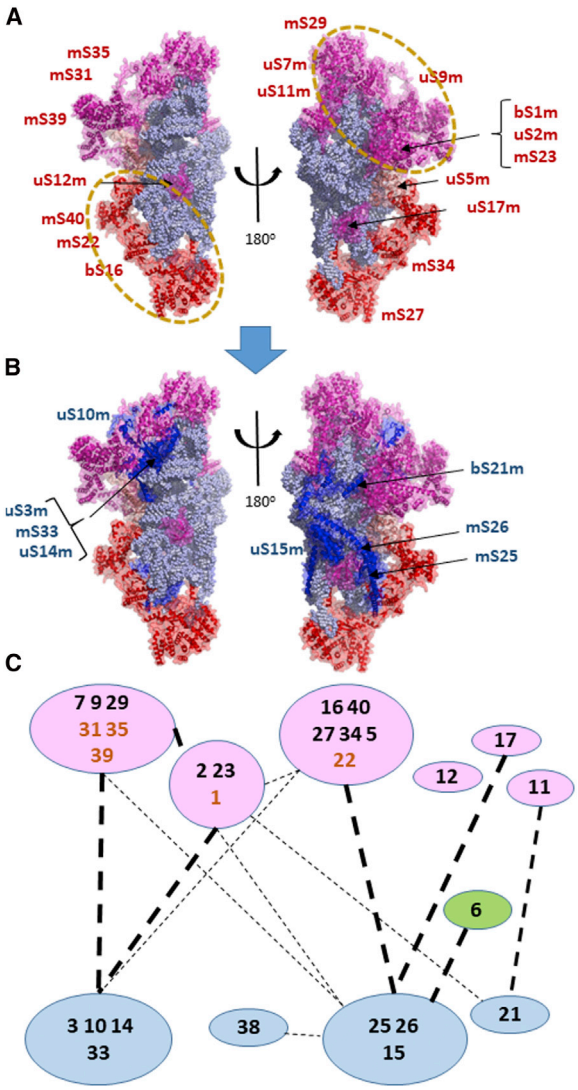

Figure 5. Assembly Scheme for the SSU

The early- and late-binding MRPs are illustrated in (A) and (B), respectively, from two points of view, one rotated 180° with respect to the other. The 12S rRNA is shown with light blue spheres representing individual residues. Proteins are shown as cartoon structures within transparent surfaces.

(A) Early MRPs are shown in magenta and, for the group containing mS27, in red. uS5m is shown in a salmon color to indicate that it bridges the upper and lower groups, which are outlined by dashed circles and illustrated in greater detail in Figure S5.

(B) Late-binding proteins are shown in blue along with the early proteins as in (A).

(C) The assembly scheme for the SSU showing protein-protein interactions between individual or grouped polypeptides, with their longer standard names truncated to numbers for simplicity. Heavy dashed lines indicate interaction surface areas greater than 1,000 Å^2 (see Figure S4), while lighter dashed lines indicate interactions between 1,000 Å^2 and 350 Å^2. mS22, mS31, mS35, mS39, and bS1m are shown in boldface brown type, since they are early-binding proteins lacking extensive RNA contacts. Since they depend on other proteins for assembly, they may be considered secondary binding proteins associated with the indicated early clusters. uS6m and mS38 are shown as independent proteins with variable association with the mS26 group but did not yield sufficient proteomic data for definitive kinetic assignment.

surface of 1,797 Å^2 with uS2m as well as a substantial interaction with bS1m (Figure S5D). This module interacts strongly with early proteins uS9m and uS5m. Remaining early proteins uS11m, uS12m, and uS17m bind as individual proteins in the center (Figure 5A). Since these three proteins do not contact other early-binding proteins, their addition appears to depend upon their substantial interactions with 12S rRNA (Figure S3). Late-binding proteins also showed some tendency to cluster, with one group (uS14m, uS10m, uS3m, and mS33) binding in the head region in association with the early uS7m-mS29 group. The significant contrast in the assembly kinetics displayed by the early-binding uS7-mS29 group (Figure S5C) and the late-binding uS3m group (Figure S5E) suggests that the former recruits the latter. A second set of late-binding proteins, uS15m, mS25, and mS26, joins the body near the early bS16m-mS22 complex. The superficial location and late-binding kinetics of uS15m, mS25, and mS26 qualify these as tertiary binding proteins dependent on the presence of early proteins with which they interact, including members of the bS16m-mS22 set as well as uS9m and uS17m. It is notable that the early proteins all have a substantial presence in the nucleoid fraction (Bogenhagen et al., 2014) and bind to the outer surface of the SSU, away from the interface with the LSU. In contrast, the late-binding proteins (blue in Figure 5B) tend to localize closer to the interface with the LSU.

LSU Assembly

The earliest proteins to bind 16S rRNA include 24 proteins, some of which have very extensive RNA contacts (Figure S3), including bL20 and two pairs that extend deeply into the 16S rRNA, uL3m-bL19m and uL4m-uL15m. The working model for LSU assembly (Figures 6 and 7) features subgroups of proteins with strong interactions (Figures S4B, S6, and S7). However, there are few strong interactions between these subgroups. The similar assembly kinetics displayed by these three early-binding modules is consistent with the possibility that the proteins within each subgroup bind the structure in a coordinated manner. Some early-binding groups surprisingly include proteins that have no direct contact with RNA, such as mL39 and mL50, like early-binding SSU proteins mS22, mS31, mS35, and mS39. mL50 is recruited as an early-binding protein by its substantial interactions with the uL4m-uL15m heterodimer and mL49. Similarly, a group with broad-based mutual interactions, uL3m, bL19m, uL14m, bL17m, uL22m, and bL32m, appears to anchor binding of mL39 and, later, mL45, which also has minimal direct RNA contact. The incorporation of mL45 at an early stage may serve to tether the 39S subunit at the inner membrane during subsequent steps in assembly (Englmeier et al., 2017; Greber et al., 2014).

A number of early-binding proteins associate closely with tRNA^V in the central protuberance of the 39S subunit, raising the prospect that they may serve to retain the tRNA in the structure at an early stage. There are two possible sources for the tRNA in the structure. Either it is recruited from a free pool of tRNAs or the copy of tRNA^V or tRNA^F that is co-transcribed with 12S and 16S rRNA is built into the mitoribosome. The latter possibility seems more likely, since only tRNAs adjacent to 12S rRNA are incorporated into the mitoribosome. However, this would require a large-scale relocation of the nascent tRNA^V to a position far from its location in the primary transcript, since it

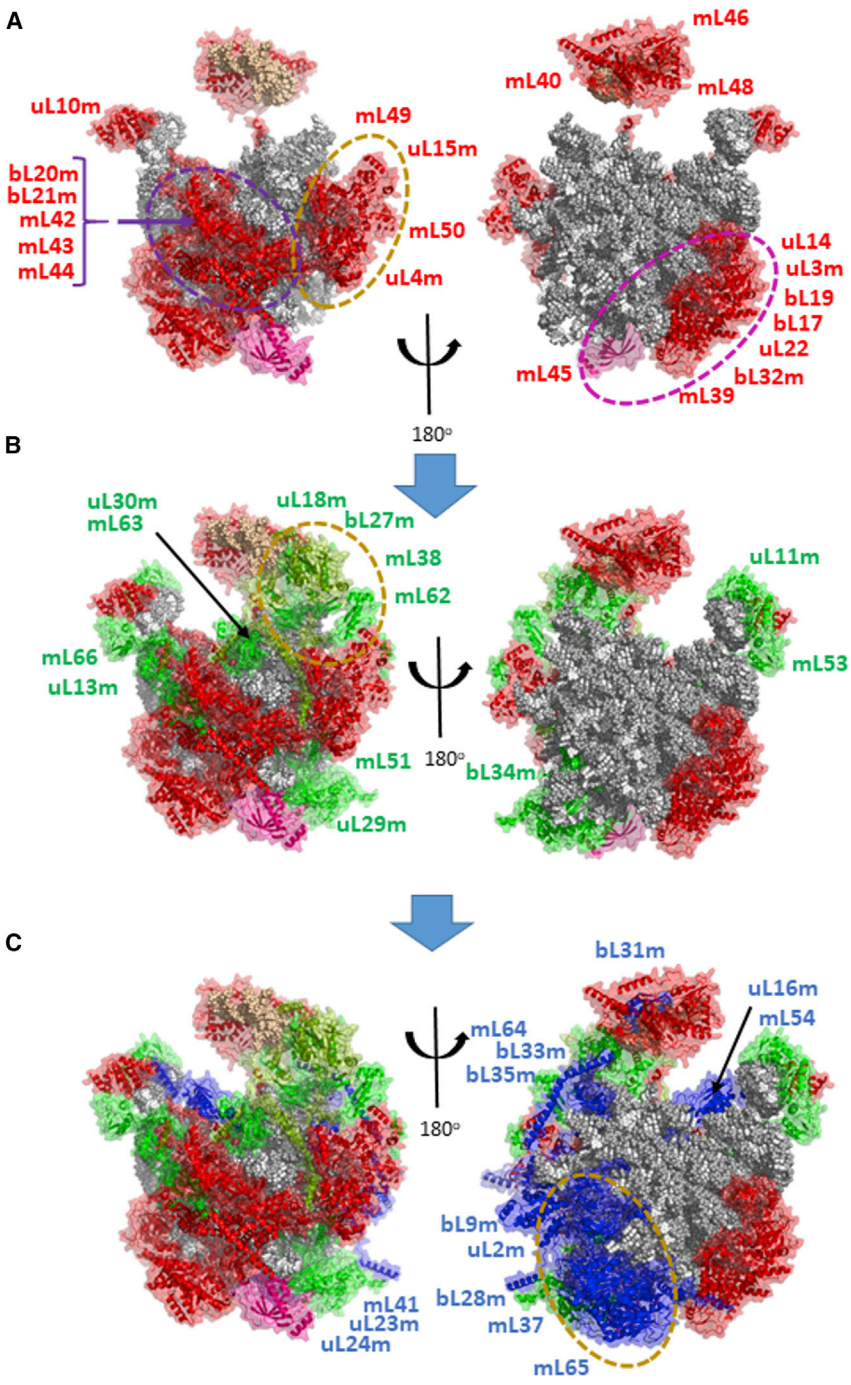

Figure 6. Model for Assembly of the LSU

16S rRNA and $tRNA^{V}$ are shown with spheres representing individual residues in gray or tan, respectively. Proteins are shown as cartoon structures within transparent surfaces. Major clusters of coordinately assembled interacting proteins are surrounded by dashed ovals and illustrated in Figures S6 and S7.

(A) Early MRPs are shown in red, but with mL45 shown in magenta to provide a marker

(B) Intermediate proteins are shown in green, but uL18m and mL63 are colored pea green, since they exhibit earlier binding kinetics than other intermediate proteins.

(C) Late-binding proteins are shown in blue.

is not found near the 5′ end of 16S rRNA in the LSU. How the tRNA is retained in the structure during assembly is not known. In the final mitoribosome structure, the tRNA is nestled between two groups of proteins (Figures 6 and S7B) that have roughly similar incorporation kinetics. One group of proteins with strong mutual interactions, mL40, mL46, and mL48, binds one facet of the tRNA, while a second group containing mL38, uL18m, and bL27m binds the other. The incorporation kinetics for these proteins suggest that the mL40-46-48 group binds at a slightly earlier stage along with mL38, while bL27m, uL18m, and mL62 bind slightly later (Figure S7B). The assembly of the central protuberance presents a structural problem not observed elsewhere in the mitoribosome. The three proteins on one side of the tRNA binding pocket, mL40, mL46, and mL48, all share extensive binding surfaces with bL31m, but bL31m behaved as a late-binding protein in our SILAC data (Figures S7A and S7B). bL31m is rather firmly enclosed by these three proteins in the final cryo-EM structure. Future experiments may shed light on the question of whether the mL40-46-48 trimer is sufficiently flexible to incorporate bL31m at a later stage in assembly.

Overall, 21 of the 24 early-binding LSU proteins are members of four large clusters that also share some weaker binding interactions. All of these clusters contain proteins with high enrichment of nascent protein in the nucleoid fraction (Bogenhagen et al., 2014). Together, the early proteins form a nearly complete band decorating a swath of outer surface of the LSU but largely avoiding the intersubunit face (Figure 6). Interestingly, a recent cryo-EM analysis of late-stage 39S subunit assembly intermediates has also found that the morphology of the intersubunit interface is well organized and well resolved only at a late stage in assembly (Brown et al., 2017).

Intermediate-binding LSU proteins reside in a more scattered distribution on the 39S subunit, often sharing interactions with early-binding proteins (Figure 6B). uL13m-mL66, with a BSA of 2,312 $Å^2$, bind the L10 stalk through interactions with RNA as well as early-binding proteins. These two proteins and uL11m tend to surround uL10m. A major set of intermediate-late proteins (mL41, uL23m, uL24m, uL29, and bL34m) joins the base of the LSU to contribute to the formation of the peptide exit tunnel (Figure S7C). These proteins make few contacts to early

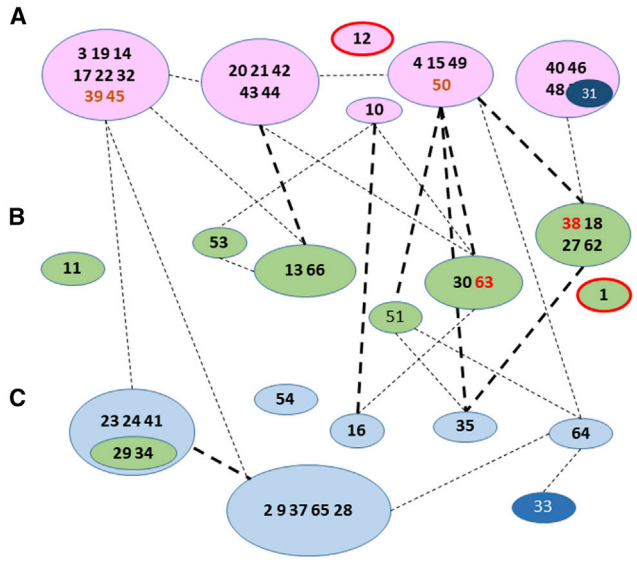

Figure 7. Scheme for Assembly of the LSU

Assembly scheme showing protein-protein interactions between individual or grouped polypeptides with line designations based on Figure S4 as in Figure 5C and with the longer standard names of individual proteins truncated to numbers for simplicity. uL12m and uL1m are included in the early and intermediate groups based on the kinetic proteomic results but are outlined in red, since they were not identified in the cryo-EM structure. bL31m is shown as an atypical member of an early group that appears to join the structure at a later stage (see text for details). mL39, mL45, and mL50 are shown in boldface brown type, since they are early-binding proteins but do not have extensive RNA contacts. Since they depend on other proteins for assembly, they may be considered secondary binding proteins. mL38 and mL63 are shown in boldface red type, since their assembly kinetics resemble those of early-binding proteins, but they have very close associations with intermediate binding proteins. uL29m and bL34m are shown within a green ellipse associated with a late group, since they showed somewhat earlier assembly kinetics than other group members.

proteins or to other intermediate proteins. They likely bind to an RNA surface that becomes available only after rearrangement of the 16S RNA structure following binding of early proteins.

At a later assembly stage, uL2m, mL37, and mL65 join the structure to add a prominent mass adjacent to uL23m:uL29m approaching the interface of the LSU with the SSU (Figures 6C and S7D), where uL2m forms one of the intersubunit bridges (to bS6m). mL37 joins bL28m in extended contacts wrapping along intermediate-binding protein uL29. mL37 and mL65 share a substantial protein-protein interface and serve to compensate for a large evolutionary RNA deletion in domain III of the LSU rRNA (Brown et al., 2014). This pair continues the theme that some proteins that are tightly associated with one another and join the structure at approximately the same stage may bind in a coordinate manner. uL2m is of particular interest, since it shares a relatively large interaction surface with 16S rRNA (Figure S3), but it was not observed at nucleoids. We do not know what prevents binding of uL2m during early stages of mitoribosome assembly, but we suggest that its binding requires RNA conformational changes induced by the binding of primary MRPs.

DISCUSSION

The mitoribosome differs from the bacterial ribosome in its high ratio of protein to RNA as described in elegant recent cryo-EM studies (Amunts et al., 2015; Greber et al., 2015). The assembly of the mammalian mitoribosome is a poorly studied, complex process requiring independent synthesis and mitochondrial import of 82 structural proteins. We report results of an extensive series of SILAC pulse-labeling experiments revealing great variability in the kinetics of appearance of MRPs in intact mitoribosomes. We considered several factors that might contribute to this variability, including the exchange of nascent MRPs into previously assembled mitoribosomes. We found that this mechanism can explain the rapid appearance of one MRP, bL33m, in mitoribosomes, but no others. We also considered the possibility that some MRPs may exhibit delayed assembly because newly imported nascent copies may be diluted by large pools of previously synthesized, unlabeled proteins. We concluded that this was a minor contributing factor, since we found that some of the proteins that assemble slowly do not have large pools of free protein. Thus, we consider that SILAC can distinguish between MRPs that participate at early and late stages in mitoribosome assembly. Interestingly, several MRPs implicated to date in serious mitochondrial disorders participate at early stages in mitoribosome assembly, including uL3, mL44, uS7m, mS22, and uS16m (Baertling et al., 2015; Carroll et al., 2013; Distelmaier et al., 2015; Emdadul Haque et al., 2008; Menezes et al., 2015; Miller et al., 2004; Saada et al., 2007; Smits et al., 2011). Lack of an early-binding protein may be more likely to disrupt mitoribosome structure and subsequent steps in assembly.

Our results (Figure 2) suggested that complete assembly requires ~2–3 hr, and additional pulse-chase labeling experiments confirmed that early-binding pulse labeled MRPs can be effectively "chased" into completed mitoribosomes (Figure 3). Expanding our pulse-chase SILAC approach to study the entire mitochondrial pool of MRPs (free plus assembled copies) revealed that most MRPs are synthesized and imported in considerable excess over the amount required to support assembly. This influx of nascent MRPs provides a supply of parts for mitoribosome assembly, but the accessibility of the proper proteins exactly when required may still limit the overall pace of assembly. We found that unassembled copies of MRPs are degraded relatively rapidly. This turnover may be essential to degrade MRPs imported into mitochondria not actively involved in mitoribosome assembly to avoid excessive accumulation. These results have important implications for mitochondrial proteostasis and quality control that may be explored in future experiments (Rugarli and Langer, 2012).

An additional factor that may contribute to the apparently long duration required for mitoribosome assembly is the unusual extent to which this must be coordinated with mtRNA processing events. The mitochondrial rRNAs are tandemly transcribed to generate a precursor termed RNA 4 (Gelfand and Attardi, 1981) containing 12S-tRNA^{V}-16S RNA and possibly tRNA^{F} that is cleaved by RNase P and ELAC2 to separate the mature RNAs. These incisions, led by RNase P, are not necessarily rapid steps, as evidenced by the facile detection of the RNA 4 precursor. mtRNA processing is clearly essential for mitoribosome

assembly, as illustrated by the deleterious effects on mitoribosome assembly resulting from genetic inactivation of the RNase P nuclease, MRPP3 (Rackham et al., 2016). It will be important to determine how potential impairment of RNase P activity may contribute to the clinical impact of mutations in RNase P subunit genes (Alsmadi et al., 2009; Zschocke, 2012). Since RNA processing and protein-RNA binding occur in the same compartment and the RNA scaffold lacks extragenic spacer regions it is important that early-binding MRPs should not block cleavage by RNase P or RNase Z, or access of RNA modification enzymes. Our previous finding that SSU MRPs are more abundant in nucleoid preparations than LSU proteins (Bogenhagen et al., 2014) implies that SSU assembly may progress further than LSU assembly before either intermediate is liberated from the nucleoid and transferred to a nearby RNA granule (Jourdain et al., 2016), where mitoribosome assembly is thought to continue. Super-resolution structured illumination microscopy (SIM) and stochastic optical reconstruction microscopy (STORM) imaging shows that most RNA granules in cultured HeLa cells are in intimate contact with nucleoids to facilitate this transfer (D.F.B., unpublished data).

SILAC labeling suggested a temporal hierarchy for mitoribosome assembly events. Examination of the roster of early-binding MRPs identified numerous examples of sets of proteins that shared both similar binding kinetics and extensive buried surface areas (BSAs) in the final structure. Detailed analysis of protein-protein and protein-RNA interactions identified twelve instances where three or more very closely associated proteins join the complex at the same stage in assembly, along with two other closely linked pairs. These coordinately assembled modules represent 60 of the 82 MRPs, indicating that protein-protein interactions have a far greater relative importance in assembly of the mitoribosome than in the bacterial ribosome. In both systems, assembly is rather probabilistic in nature as it characterizes a general landscape of protein binding that most likely does not follow a strictly ordered sequence of events. Coordinated assembly appears to be necessary to recruit eight proteins that bind at early stages in mitoribosome assembly but lack substantial contact with rRNAs, including mS22, mS31, mS35, mS39, bS1m, mL39, mL50, and mL45. Mitoribosome assembly would be facilitated by association of MRPs in pre-assembled sub-complexes, as has been documented for assembly of mammalian respiratory complex I (Guerrero-Castillo et al., 2017). While this is not absolutely required for coordinated assembly, the model generated by our SILAC labeling approach provides a guide for future experiments to search for such intermediates and to dissect the assembly sequence in greater detail.

EXPERIMENTAL PROCEDURES

Cell Culture and Mitoribosome Preparation

HeLa cell culture, SILAC pulse labeling, and mitochondrial isolation were conducted as described previously (Bogenhagen et al., 2014; Lee and Bogenhagen, 2016). Each preparation typically started with ~1.5 to 2 × 10^8 adherent cells. Mitochondrial lysis and mitoribosome preparation followed Matthews and O'Brien (Matthews et al., 1982) as adapted by Brown et al. (2014) to permit mitochondrial isolation and mitoribosome purification within 24–26 hr without freezing. Detailed procedures are in Supplemental Experimental Procedures.

Peptide Identification and Quantification by LC-MS/MS

Trypsin digestion and LC-MS/MS analysis of peptides was performed using standard methods as described in Supplemental Experimental Procedures.

Statistical Methods of Data Analysis

Peptide data produced by SCIEX Protein Pilot software in text file format was imported into Excel and searched to select only peptides derived from human MRPs. In some experiments, results were filtered for all mitochondrial proteins in the Mitocarta 2.0 collection (Calvo et al., 2016). Peptides were sorted to eliminate those with low heavy or light peptide signals, confidence scores <90%, and those that might represent another peptide. Peptides with inappropriately high H:L ratios in the highest 2.5% of the distribution were manually removed as outliers. Peptide information was imported into SAS JMP 13 software to generate average H:L ratios and SE calculations using robust fitting (Huber, 1973). Tests of statistical significance used one-way ANOVA with pairwise Student's t test. Structural renderings were generated using Pymol.

SUPPLEMENTAL INFORMATION

Supplemental Information includes Supplemental Experimental Procedures, seven figures, three tables, and two datasets and can be found with this article online at https://doi.org/10.1016/j.celrep.2018.01.066.

ACKNOWLEDGMENTS

D.F.B. would like to acknowledge the accomplishments of his Stony Brook University colleague Dr. Melvin Simpson in making the first observations of translation in mitochondria and reaching his 96th birthday. This work was supported by grants to D.F.B. from NIH (1R01GM112790) and the United Mitochondrial Disease Foundation.

AUTHOR CONTRIBUTIONS

D.F.B. performed all cell labeling, fractionation, and preparation of samples for proteomic analysis with technical assistance from A.G.O.-F. J.D.H. performed protein digestion and LC-MS/MS analysis. J.D.H. and D.F.B. analyzed proteomic data. M.G.-D. and D.F.B. conducted the structural biology analyses and wrote the paper.

DECLARATION OF INTERESTS

The authors declare no competing interests.

Received: June 1, 2017
Revised: November 1, 2017
Accepted: January 22, 2018
Published: February 13, 2018

REFERENCES

Alsmadi, O., Muiya, P., Khalak, H., Al-Saud, H., Meyer, B.F., Al-Mohanna, F., Alshahid, M., and Dzimiri, N. (2009). Haplotypes encompassing the KIAA0391 and PSMA6 gene cluster confer a genetic link for myocardial infarction and coronary artery disease. Ann. Hum. Genet. *73*, 475–483.

Amunts, A., Brown, A., Bai, X.C., Llácer, J.L., Hussain, T., Emsley, P., Long, F., Murshudov, G., Scheres, S.H.W., and Ramakrishnan, V. (2014). Structure of the yeast mitochondrial large ribosomal subunit. Science *343*, 1485–1489.

Amunts, A., Brown, A., Toots, J., Scheres, S.H.W., and Ramakrishnan, V. (2015). Ribosome. The structure of the human mitochondrial ribosome. Science *348*, 95–98.

Anderson, S., Bankier, A.T., Barrell, B.G., de Bruijn, M.H.L., Coulson, A.R., Drouin, J., Eperon, I.C., Nierlich, D.P., Roe, B.A., Sanger, F., et al. (1981). Sequence and organization of the human mitochondrial genome. Nature *290*, 457–465.

Baertling, F., Haack, T.B., Rodenburg, R.J., Schaper, J., Seibt, A., Strom, T.M., Meitinger, T., Mayatepek, E., Hadzik, B., Selcan, G., et al. (2015). MRPS22

mutation causes fatal neonatal lactic acidosis with brain and heart abnormalities. Neurogenetics *16*, 237–240.

Bahadur, R.P., Chakrabarti, P., Rodier, F., and Janin, J. (2003). Dissecting subunit interfaces in homodimeric proteins. Proteins *53*, 708–719.

Bogenhagen, D.F., Martin, D.W., and Koller, A. (2014). Initial steps in RNA processing and ribosome assembly occur at mitochondrial DNA nucleoids. Cell Metab. *19*, 618–629.

Brown, A., Amunts, A., Bai, X.C., Sugimoto, Y., Edwards, P.C., Murshudov, G., Scheres, S.H.W., and Ramakrishnan, V. (2014). Structure of the large ribosomal subunit from human mitochondria. Science *346*, 718–722.

Brown, A., Rathore, S., Kimanius, D., Aibara, S., Bai, X.C., Rorbach, J., Amunts, A., and Ramakrishnan, V. (2017). Structures of the human mitochondrial ribosome in native states of assembly. Nat. Struct. Mol. Biol. *24*, 866–869.

Calvo, S.E., Clauser, K.R., and Mootha, V.K. (2016). MitoCarta2.0: an updated inventory of mammalian mitochondrial proteins. Nucleic Acids Res. *44* (*D1*), D1251–D1257.

Carroll, C.J., Isohanni, P., Pöyhönen, R., Euro, L., Richter, U., Brilhante, V., Götz, A., Lahtinen, T., Paetau, A., Pihko, H., et al. (2013). Whole-exome sequencing identifies a mutation in the mitochondrial ribosome protein MRPL44 to underlie mitochondrial infantile cardiomyopathy. J. Med. Genet. *50*, 151–159.

Desai, N., Brown, A., Amunts, A., and Ramakrishnan, V. (2017). The structure of the yeast mitochondrial ribosome. Science *355*, 528–531.

Distelmaier, F., Haack, T.B., Catarino, C.B., Gallenmüller, C., Rodenburg, R.J., Strom, T.M., Baertling, F., Meitinger, T., Mayatepek, E., Prokisch, H., and Klopstock, T. (2015). MRPL44 mutations cause a slowly progressive multisystem disease with childhood-onset hypertrophic cardiomyopathy. Neurogenetics *16*, 319–323.

Emdadul Haque, M., Grasso, D., Miller, C., Spremulli, L.L., and Saada, A. (2008). The effect of mutated mitochondrial ribosomal proteins S16 and S22 on the assembly of the small and large ribosomal subunits in human mitochondria. Mitochondrion *8*, 254–261.

Englmeier, R., Pfeffer, S., and Förster, F. (2017). Structure of the human mitochondrial ribosome studied in situ by cryoelectron tomography. Structure *25*, 1574–1581.e2.

Gelfand, R., and Attardi, G. (1981). Synthesis and turnover of mitochondrial ribonucleic acid in HeLa cells: the mature ribosomal and messenger ribonucleic acid species are metabolically unstable. Mol. Cell. Biol. *1*, 497–511.

Greber, B.J., Boehringer, D., Leitner, A., Bieri, P., Voigts-Hoffmann, F., Erzberger, J.P., Leibundgut, M., Aebersold, R., and Ban, N. (2014). Architecture of the large subunit of the mammalian mitochondrial ribosome. Nature *505*, 515–519.

Greber, B.J., Bieri, P., Leibundgut, M., Leitner, A., Aebersold, R., Boehringer, D., and Ban, N. (2015). Ribosome. The complete structure of the 55S mammalian mitochondrial ribosome. Science *348*, 303–308.

Guerrero-Castillo, S., Baertling, F., Kownatzki, D., Wessels, H.J., Arnold, S., Brandt, U., and Nijtmans, L. (2017). The assembly pathway of mitochondrial respiratory chain complex I. Cell Metab. *25*, 128–139.

Huber, P.J. (1973). Robust regression: asymptotics, conjectures and Monte Carlo. Ann. Stat. *1*, 799–821.

Jourdain, A.A., Boehm, E., Maundrell, K., and Martinou, J.-C. (2016). Mitochondrial RNA granules: Compartmentalizing mitochondrial gene expression. J. Cell Biol. *212*, 611–614.

Kastritis, P.L., and Bonvin, A.M. (2012). On the binding affinity of macromolecular interactions: daring to ask why proteins interact. J. R. Soc. Interface *10*, 20120835.

Krissinel, E. (2010). Crystal contacts as nature's docking solutions. J. Comput. Chem. *31*, 133–143.

Lee, K.-W., and Bogenhagen, D. (2016). Scalable isolation of mammalian mitochondria for nucleic acid and nucleoid analysis. In Mitochondrial DNA, M. McKenzie, ed. (Springer), pp. 67–79.

Matthews, D.E., Hessler, R.A., Denslow, N.D., Edwards, J.S., and O'Brien, T.W. (1982). Protein composition of the bovine mitochondrial ribosome. J. Biol. Chem. *257*, 8788–8794.

Menezes, M.J., Guo, Y., Zhang, J., Riley, L.G., Cooper, S.T., Thorburn, D.R., Li, J., Dong, D., Li, Z., Glessner, J., et al. (2015). Mutation in mitochondrial ribosomal protein S7 (MRPS7) causes congenital sensorineural deafness, progressive hepatic and renal failure and lactic acidemia. Hum. Mol. Genet. *24*, 2297–2307.

Miller, C., Saada, A., Shaul, N., Shabtai, N., Ben-Shalom, E., Shaag, A., Hershkovitz, E., and Elpeleg, O. (2004). Defective mitochondrial translation caused by a ribosomal protein (MRPS16) mutation. Ann. Neurol. *56*, 734–738.

Rackham, O., Busch, J.D., Matic, S., Siira, S.J., Kuznetsova, I., Atanassov, I., Ermer, J.A., Shearwood, A.M., Richman, T.R., Stewart, J.B., et al. (2016). Hierarchical RNA processing is required for mitochondrial ribosome assembly. Cell Rep. *16*, 1874–1890.

Rugarli, E.I., and Langer, T. (2012). Mitochondrial quality control: A matter of life and death for neurons. EMBO J. *31*, 1336–1349.

Saada, A., Shaag, A., Arnon, S., Dolfin, T., Miller, C., Fuchs-Telem, D., Lombes, A., and Elpeleg, O. (2007). Antenatal mitochondrial disease caused by mitochondrial ribosomal protein (MRPS22) mutation. J. Med. Genet. *44*, 784–786.

Schwanhäusser, B., Busse, D., Li, N., Dittmar, G., Schuchhardt, J., Wolf, J., Chen, W., and Selbach, M. (2011). Global quantification of mammalian gene expression control. Nature *473*, 337–342.

Shajani, Z., Sykes, M.T., and Williamson, J.R. (2011). Assembly of bacterial ribosomes. Annu. Rev. Biochem. *80*, 501–526.

Smits, P., Saada, A., Wortmann, S.B., Heister, A.J., Brink, M., Pfundt, R., Miller, C., Haas, D., Hantschmann, R., Rodenburg, R.J.T., et al. (2011). Mutation in mitochondrial ribosomal protein MRPS22 leads to Cornelia de Lange-like phenotype, brain abnormalities and hypertrophic cardiomyopathy. Eur. J. Hum. Genet. *19*, 394–399.

Talkington, M.W.T., Siuzdak, G., and Williamson, J.R. (2005). An assembly landscape for the 30S ribosomal subunit. Nature *438*, 628–632.

Ugalde, C., Vogel, R., Huijbens, R., Van Den Heuvel, B., Smeitink, J., and Nijtmans, L. (2004). Human mitochondrial complex I assembles through the combination of evolutionary conserved modules: a framework to interpret complex I deficiencies. Hum. Mol. Genet. *13*, 2461–2472.

Zschocke, J. (2012). HSD10 disease: clinical consequences of mutations in the HSD17B10 gene. J. Inherit. Metab. Dis. *35*, 81–89.

Cell Reports, Volume *22*

Supplemental Information

Kinetics and Mechanism of Mammalian Mitochondrial Ribosome Assembly

Daniel F. Bogenhagen, Anne G. Ostermeyer-Fay, John D. Haley, and Miguel Garcia-Diaz

Supplemental Information
Supplemental Methods

Cell culture and SILAC labeling. Human HeLa cells were grown in monolayer culture in DMEM (Thermo-Fisher) supplemented with 10% fetal bovine serum (Atlantic Biologicals) and 1% penicillin-streptomycin (Thermo-Fisher). SILAC labeling (all reagents Thermo-Fisher) was done using DMEM lacking lysine/arginine made with dialyzed fetal bovine serum and supplemented with 30 mg/l $^{13}C_6$-arginine and 50 mg/l $^{13}C_6$-lysine (K6R6 medium) for the indicated labeling interval as described (Boisvert et al., 2011). Medium changes to initiate or terminate the pulse labeling involved one rinse with PBS followed by two rinses with brief (2-5 min) incubation at 37 ºC with Hanks basic salt solution.

Mitoribosome preparation. Cell lysis and mitochondrial lysis were conducted in buffers containing HALT protease/phosphatase inhibitor (Thermo-Fisher) and other buffers were supplemented with PMSF, leupeptin, and pepstatin as described (Bogenhagen et al. 2014). All steps were conducted at 4 ºC. Briefly, mitochondria were lysed in a solution containing 100 mM KCl, 20 mM $MgCl_2$, 0.8 mM EDTA, 20 mM Hepes, pH 8, 7 mM beta-mercaptoethanol, 100 μM spermine and 2% Triton X-100. Control experiments showed mtDNA nucleoids did not remain intact under these high salt conditions. Following centrifugation at 10,000 g for 5 min, the lysate was layered on a prepared step gradient containing 2 ml 10% sucrose overlayed above a 1 ml pad of 48% sucrose, both in buffer B (100 mM KCl, 20 mM $MgCl_2$, 20 mM Hepes, pH 8, 5 mM 2-mercaptoethanol, 0.5% Triton X-100) and centrifuged for 4 hr at 200,000 g in a Beckman SW60T1 rotor (11 x 60 mm). Fractions were collected from the tube bottom and mitoribosomes sedimented to the 10/48% sucrose interface were identified by SyBr Green II dye binding fluorescence. A small sample was reserved for 14% PAGE-SDS analysis with immunoblotting using antisera to human uL10m and bS15m (Proteintech 16652-1-AP and 17006-1-AP, respectively) and standard detection with a chemiluminescence assay. Fractions containing the peak of rRNA fluorescence were pooled, diluted with buffer B lacking sucrose and concentrated by ultrafiltration using a Pierce 150 kDa cutoff centrifugal ultrafiltration device (Thermo-Fisher). The retentate was layered on a continuous 10-35% sucrose gradient (11 x 60 mm) in buffer B and centrifuged at 85,000 g for 14 hr. Fractions were collected from the tube bottom and mitoribosomes were detected by immunoblotting as described above. Proteins were precipitated from the peak fractions using chloroform methanol (Wessel and Flugge, 1984) and submitted for fragmentation and mass spectrometry analysis. Other antisera used included anti-bL19m (Proteintech 16517-1-AP), mL44 (Proteintech 16394-1-AP), mL45 (Sigma HPA023373), uS17m (Proteintech 18881-1-AP), mS23 ((Proteintech 15345-1-AP) and mS27 (Proteintech 17280-1-AP).

Peptide identification and quantification by LC-tandem MS
Protein samples were dissolved in 8 M urea, 100 mM ammonium bicarbonate, sonicated for 30 sec twice and subjected to reduction (5 mM DTT), alkylation (10 mM iodoacetamide), diluted to 2 M urea and digested with trypsin at 37ºC overnight. Peptides were desalted on reverse phase resin (HLB; waters.com), lyophilized, resuspended in 0.1% formic acid and analyzed by in line cation-exchange (SCX) fractionation by nano LC-MS/MS. Parent peptide mass, collision-induced fragment mass information and isotopically-encoded peptide abundance values were obtained by liquid chromatography-electrospray ionization tandem mass spectrometry (LC-MS/MS), using an orthogonal quadruple TOF instrument (5600Plus; AB-Sciex) followed by protein database searching. Data dependent LC-MS/MS experiments were performed for each of ten fractions for SCX-C18 LC-MS/MS (load, 0, 25, 50, 75, 100, 150, 200, 300, 500 mM ammonium acetate). Proteins were identified from survey and product ion spectra data, using the Paragon algorithm of ProteinPilot (v5.01; (Shilov et al., 2007)) and GPM (v2.2.1; (Beavis, 2006)). HPLC C18 columns were prepared using a P-2000 CO_2 laser puller (Sutter Instruments) and silica tubing (75µm ID x ~10 cm) and were self-packed with 3 µm Magic AQ C18 resin (michrombioresources.com). Peptides were separated by reverse-phase HPLC with a flow rate of 200 nl/min, using a 10 min isocratic loading step 0.1% formic acid/water), a gradient elution step with acetonitrile (ACN), 0.1% formic acid (0.23%/min) over 90 min, followed by 5 min 70% ACN wash and 25 min re-equilibration steps. Electrospray ionization was achieved using spray voltage of ~2.4 kV. Information-dependent MS and MS-MS acquisitions were made using a 0.25 second survey scan (m/z 400 – 1600) followed typically by 12 consecutive second product ion scans of 0.1 seconds each (m/z 100 – 1400), using rolling collision energy. Parent ion with charge states of 2+, 3+ and 4+ were selected with a 15-second exclusion period. MS data was collected using Analyst (absciex.com). Fourfold MS and twelve fold MS/MS time binning was used to increase sensitivity. Data was collected throughout the 120-minute HPLC cycle. Raw data files will be deposited in ProteomeXchange (Vizcaino et al., 2014).

Protein and peptide identification and quantitation

Two missed tryptic cleavages were allowed and posttranslational modifications considered included cysteine derivatization, STY phosphorylation, deamidation, carbamylation, oxidation and SILAC labels. Database searches used the human UniProt FASTA database (UniProtKB/Swiss-Prot 'Homo Sapiens' subset consisted of 48036 entries; 3-2016; http://www.uniprot.org). When multiple protein isoforms were identified, Protein Pilot allowed only peptides specific to each detected isoform to be used, which factored in ion counts for weighting in the protein ratio calculation. Parsimony of protein results was assured by rigorous protein inference with the ProGroup algorithm. False discovery rates of peptide capture experiments were <1%. For statistical analysis using peptide data we required 4 or more peptides with individual peptide assignments at >90% confidence, where both light and heavy intensity values were measured. Peptide peak areas were normally distributed by log10 + 1 conversion followed by paired t-test. 'Digital peptides' where only light or heavy peptides were measured were considered separately and not assigned ratios of 0.01 or 100.

Kinetic model for H:L labeling of MRPs

Considerations: Cells in exponential growth are initially unlabeled with stable isotopes until the start of a variable labeling period of t hours. Cells are thoroughly washed and provided with medium containing stable-isotope labeled Arg_6, Lys_6 to initiate the pulse. We assume the conversion of amino acid pools occurs rapidly (Zhang et al., 2014). We take as given that newly synthesized proteins accumulate to support cell growth AND to replace any protein degraded (turned over) during the labeling interval. The simple model assumes there is not a substantial pool of free mitoribosomal subunits available for assembly, but deviation from predicted behavior may indicate this assumption is not correct for all MRPs.

Terms:

T_g=cell doubling time for exponential growth

$t_{1/2}$= half-life of preexisting protein

$R(t)$ = total mitoribosomal protein at time t

$R_L(t)$ = total light mitoribosomal protein at time t

$R_H(t)$ = total heavy (newly synthesized) protein at time t

$$R(t) = R_L(t) + R_H(t)$$

Total mitoribosomes increase in number along with cell growth

$$R(t) = R(0)e^{\ln 2 * t/Tg}$$

note $R_L(0)=R(0)$ and will only decrease during the pulse following turnover

New synthesis during the pulse generates heavy mitoribosome proteins. These can also be subject to turnover, but in a continuous labeling experiment will also be replaced by other newly synthesized proteins to maintain the total population of mitoribosomes. Thus, any turnover of newly synthesized mitoribosomal proteins has no effect on $R_H(t)$.

$R_H(t)$ = all mitoribosomal protein copies that are not light

$R_H(t)$ = (total mitoribosomes)-(those pre-existing before the pulse)

$$R_H(t) = R(t) - R_L(0)\, e^{\ln 2 * t/Tg}$$

Recall $R(0) = R_L(0)$

LC-MS/MS measures the H/L ratio

$$R^H/_L = R_H(t)/R_L(t)$$

then

$$R^H/_L = (R(0)e^{\ln 2 * t/Tg} - R_L(0)e^{\ln 2 * t/t1/2})/R_L(0)e^{\ln 2 * t/t1/2}$$

In the special case where an assembled MRP is very stable, $e^{\ln 2 * t/t1/2}$ approaches a value of $e^0=1$

$R^H/_L$ simplifies to

$$R^H/_L = e^{\ln 2 * t/Tg} - e^{\ln 2 * t/t1/2} \text{ or } e^{\ln 2 * t/Tg} - 1$$

This curve was evaluated to plot the dashed lines in Fig. 2.

In general,

$$R^{H}/_{L} = R(0)\,[e^{\ln 2 * t/Tg} - R_{L}(0)e^{\ln 2 * t/t1/2}] / R_{L}(0)e^{\ln 2 * t/t1/2}$$

$$R^{H}/_{L} = (e^{\ln 2 * t/Tg} - R_{L}(0)e^{\ln 2 * t/t1/2}) / e^{\ln 2 * t/t1/2}$$

since t and T_g are known, this can be solved for $t_{1/2}$.

Supplemental References

Beavis, R.C. (2006). Using the global proteome machine for protein identification. Methods Mol Biol *328*, 217-228.

Boisvert, F.-M., Ahmad, Y., Gierliński, M., Charrière, F., Lamont, D., Scott, M., Barton, G., and Lamond, A.I. (2011). A quantitative spatial proteomics analysis of proteome turnover in human cells. Molecular & Cellular Proteomics *11*, M111.011429.

Shilov, I.V., Seymour, S.L., Patel, A.A., Loboda, A., Tang, W.H., Keating, S.P., Hunter, C.L., Nuwaysir, L.M., and Schaeffer, D.A. (2007). The Paragon Algorithm, a Next Generation Search Engine That Uses Sequence Temperature Values and Feature Probabilities to Identify Peptides from Tandem Mass Spectra. Molecular & Cellular Proteomics *6*, 1638-1655.

Vizcaino, J.A., Deutsch, E.W., Wang, R., Csordas, A., Reisinger, F., Rios, D., Dianes, J.A., Sun, Z., Farrah, T., Bandeira, N.*, et al.* (2014). ProteomeXchange provides globally coordinated proteomics data submission and dissemination. Nature biotechnology *32*, 223-226.

Wessel, D., and Flugge, U.I. (1984). A method for the quantitative recovery of protein in dilute solution in the presence of detergents and lipids. Anal Biochem *138*, 141-143.

Zhang, T., Price, J.C., Nouri-Nigjeh, E., Li, J., Hellerstein, M.K., Qu, J., and Ghaemmaghami, S. (2014). Kinetics of precursor labeling in stable isotope labeling in cell cultures (SILAC) experiments. Anal Chem *86*, 11334-11341.

	3 Hour			4 Hour			6 Hour			12 Hour			Class
Protein	Pep	Mean	SE	Pep	Mean	SE	Pep	Mean	SE	Pep	Mean	SE	
uL1m	106	0.0552	0.0024	108	0.0895	0.0034	165	0.1557	0.0032	180	0.3663	0.0046	B
uL2m	165	0.1020	0.0026	142	0.1234	0.0041	179	0.199	0.0035	176	0.4695	0.0065	C
uL3m	61	0.0492	0.0027	114	0.0743	0.0037	97	0.108	0.0036	217	0.3341	0.0048	A
uL4m	63	0.0359	0.0029	102	0.0577	0.0031	177	0.1214	0.0043	174	0.3215	0.0044	A
bL9m	122	0.0640	0.0021	113	0.0909	0.0036	130	0.1576	0.0039	137	0.4158	0.0062	B
uL10m	42	0.0486	0.0044	40	0.0575	0.0037	58	0.1097	0.0052	86	0.2855	0.0062	A
uL11m	221	0.0655	0.0018	157	0.0893	0.0025	190	0.1551	0.0022	237	0.3876	0.0047	B
bL12m	125	0.0289	0.0017	91	0.0404	0.0024	105	0.0876	0.0038	145	0.2295	0.0050	A
uL13m	153	0.0615	0.0019	169	0.0908	0.0026	201	0.1595	0.0024	174	0.4110	0.0048	B
uL14m	66	0.0456	0.0026	55	0.0690	0.0042	64	0.1317	0.004	88	0.3902	0.0063	A
uL15m	156	0.0359	0.0017	214	0.0607	0.0025	237	0.1065	0.0025	336	0.3208	0.0037	A
uL16m	138	0.1079	0.0027	93	0.1324	0.0049	115	0.2149	0.004	100	0.4994	0.0079	C
bL17m	111	0.0372	0.0021	87	0.0678	0.0035	93	0.1253	0.0036	205	0.3611	0.0040	A
uL18m	71	0.0596	0.0036	64	0.0880	0.0045	73	0.1414	0.0044	100	0.3851	0.0067	B
bL19m	91	0.0447	0.0032	97	0.0530	0.0024	147	0.1015	0.0031	169	0.3251	0.0046	A
bL20m	36	0.0395	0.0048	52	0.0390	0.0028	64	0.1036	0.0052	75	0.3152	0.0061	A
bL21m	79	0.0345	0.0024	66	0.0605	0.0033	71	0.1027	0.0038	149	0.3276	0.0055	A
uL22m	87	0.0459	0.0026	158	0.0699	0.0026	97	0.1055	0.0029	144	0.3496	0.0048	A
uL23m	70	0.0767	0.0033	62	0.1040	0.0059	86	0.1597	0.0046	60	0.4067	0.0069	C
uL24m	212	0.0725	0.0016	135	0.1173	0.0030	151	0.182	0.0032	239	0.4352	0.0056	C
bL27m	43	0.0570	0.0035	87	0.0961	0.0042	67	0.1465	0.0039	83	0.4072	0.0074	B
bL28m	175	0.0750	0.0017	129	0.1030	0.0034	155	0.1819	0.0036	250	0.4312	0.0049	C
uL29m	135	0.0550	0.0016	119	0.0886	0.0030	140	0.1395	0.0029	149	0.3963	0.0064	B
uL30m	42	0.0643	0.0039	25	0.0708	0.0063	44	0.1265	0.0049	105	0.3526	0.0049	B
bL31m	37	0.0718	0.0040	35	0.1097	0.0066	27	0.1771	0.0091	78	0.4803	0.0083	C
bL32m	12	0.0486	0.0097	27	0.0713	0.0067	38	0.1086	0.0046	58	0.3509	0.0091	A
bL33m	16	0.2097	0.0118	17	0.2899	0.0111	12	0.4782	0.0236	14	1.1153	0.0408	C
bL34m	34	0.0633	0.0067	40	0.0774	0.0036	24	0.1414	0.0103	93	0.3866	0.0063	B
bL35m	44	0.0920	0.0040	47	0.1243	0.0056	70	0.2141	0.0048	32	0.4905	0.0132	C
mL37	280	0.0755	0.0015	251	0.0975	0.0023	308	0.1777	0.0022	371	0.4639	0.0043	C
mL38	149	0.0411	0.0020	169	0.0628	0.0022	173	0.1166	0.003	225	0.3279	0.0046	A
mL39	85	0.0352	0.0032	95	0.0561	0.0041	122	0.0907	0.0034	221	0.2829	0.0036	A
mL40	69	0.0535	0.0025	77	0.0633	0.0034	102	0.1242	0.0034	94	0.3599	0.0062	A
mL41	106	0.0762	0.0028	71	0.0978	0.0044	88	0.1699	0.0039	68	0.4302	0.0072	C
mL42	6	0.0260	0.0152	5	0.0392	0.0088	14	0.0929	0.0117	28	0.3213	0.0101	A
mL43	62	0.0416	0.0036	68	0.0649	0.0037	125	0.1047	0.0029	123	0.3125	0.0052	A
mL44	91	0.0362	0.0026	92	0.0557	0.0032	172	0.1008	0.0027	172	0.3091	0.0036	A
mL45	117	0.0507	0.0025	109	0.0733	0.0037	158	0.1104	0.0025	248	0.3346	0.0040	A
mL46	66	0.0385	0.0030	57	0.0679	0.0049	65	0.1055	0.005	133	0.2909	0.0061	A
mL48	57	0.0556	0.0035	84	0.0711	0.0031	70	0.1356	0.0041	82	0.3661	0.0076	A
mL49	98	0.0371	0.0023	113	0.0590	0.0027	110	0.1144	0.0032	171	0.3475	0.0067	A
mL50	33	0.0334	0.0056	40	0.0474	0.0043	59	0.0822	0.0031	95	0.2831	0.0060	A
mL51	19	0.0651	0.0074	28	0.0730	0.0065	10	0.1518	0.0095	42	0.4005	0.0125	B
mL53	37	0.0610	0.0059	50	0.0824	0.0052	68	0.1345	0.0041	63	0.3630	0.0071	B
mL54	8	0.0810	0.0208	14	0.0907	0.0104	11	0.152	0.0084	33	0.3463	0.0104	C
mL62	52	0.0531	0.0042	62	0.0926	0.0047	114	0.1514	0.0038	135	0.3931	0.0073	B
mL63	22	0.0466	0.0069	26	0.0750	0.0077	33	0.1244	0.0063	41	0.3840	0.0129	A
mL64	74	0.0801	0.0033	96	0.1006	0.0040	111	0.179	0.0033	153	0.4431	0.0062	C
mL65	200	0.0801	0.0022	121	0.1076	0.0035	169	0.1827	0.003	202	0.4615	0.0068	C
mL66	107	0.0598	0.0022	51	0.0864	0.0042	80	0.1534	0.0038	140	0.3535	0.0049	B

bL33m, mL52 omitted

Table S1

	3 Hour			4 Hour			6 Hour			12 Hour			Class
Protein	Pep	Mean	SE	Pep	Mean	SE	Pep	Mean	SE	Pep	Mean	SE	
bS1m	18	0.0486	0.0091	5	0.0695	0.0293	17	0.105	0.0199	34	0.1490	0.0075	A
uS2m	33	0.0492	0.0051	23	0.0801	0.0121	26	0.0933	0.0089	73	0.2373	0.0076	A
uS3m	9	0.0893	0.0175	9	0.1399	0.0166	11	0.2182	0.0131	18	0.4301	0.0152	C
uS5m	55	0.0586	0.0044	53	0.0674	0.0055	16	0.0991	0.017	154	0.2151	0.0048	A
uS7m	24	0.0372	0.3300	35	0.0607	0.0071	17	0.0856	0.0145	73	0.2103	0.0067	A
uS9m	13	0.0506	0.0149	20	0.0749	0.0155	18	0.0721	0.011	93	0.1612	0.0059	A
uS10m	6	0.0422	0.0210	4	0.0978	0.0291	8	0.1267	0.0132	51	0.3013	0.0099	C
uS11m	6	0.0330	0.0155	13	0.0410	0.0036	9	0.1144	0.0135	19	0.2801	0.0117	A
uS12m	10	0.0517	0.0115	13	0.0698	0.0060	20	0.1203	0.0086	29	0.2795	0.0095	A
uS14m	17	0.1184	0.0141	42	0.1697	0.0080	25	0.2358	0.0105	57	0.5215	0.0117	C
uS15m	67	0.0812	0.0043	56	0.1018	0.0055	29	0.1568	0.0105	93	0.3341	0.0078	C
bS16m	10	0.0322	0.0096	10	0.0449	0.0088	11	0.0711	0.0071	37	0.1367	0.0052	A
uS17m	13	0.0376	0.0129	13	0.0404	0.0078	11	0.0523	0.0047	20	0.1588	0.0060	A
bS21m	28	0.0996	0.0057	13	0.1262	0.0153	8	0.1833	0.0204	19	0.4744	0.0194	C
mS22	68	0.0423	0.0033	38	0.0666	0.0085	26	0.1002	0.0134	129	0.1593	0.0043	A
mS23	23	0.0436	0.0076	34	0.0701	0.0078	23	0.083	0.0043	48	0.2035	0.0057	A
mS25	21	0.0494	0.0066	9	0.1240	0.0156	2	0.0732	0.0129	42	0.1881	0.0082	C
mS26	14	0.0512	0.0137	13	0.1093	0.0311	4	0.1204	0.0322	66	0.1549	0.0061	C
mS27	44	0.0432	0.0037	55	0.0623	0.0055	25	0.0891	0.0107	116	0.1749	0.0039	A
mS29	39	0.0392	0.0042	45	0.0629	0.0075	27	0.0838	0.0119	99	0.1991	0.0049	A
mS31	22	0.0308	0.0061	24	0.0592	0.0091	13	0.0726	0.0077	87	0.1976	0.0044	A
mS33	12	0.0703	0.0082	22	0.1077	0.0064	22	0.1892	0.0107	14	0.4042	0.0405	C
mS34	13	0.0316	0.0108	29	0.0514	0.0072	11	0.0795	0.0201	64	0.1519	0.0054	A
mS35	34	0.0451	0.0035	28	0.0581	0.0062	25	0.1065	0.0074	69	0.3199	0.0073	A
mS39	100	0.0553	0.0019	68	0.0653	0.0050	57	0.0912	0.0054	178	0.2377	0.0039	A
mS40	17	0.0405	0.0072	9	0.0706	0.0118	7	0.0806	0.0072	39	0.2174	0.0081	A

bS6m, bS18m, mS37, mS38 omitted

Table S1. Accumulation of newly synthesized MRPs in mature ribosomes as a function of SILAC labeling time, related to Figure 2. H:L ratios observed for high quality peptide hits representing MRPs in independent triplicate pulse labeling experiments after 3, 4, 6 or 12 hr incubations in K6R6 medium. For each protein at each time point, the number of peptides considered (Pep), mean H:L ratio and standard error (SE) are shown. Cells are color-coded using conditional formatting to identify values more than one standard deviation above (yellow) or below (red) the mean for each subunit at each time interval. Proteins were assigned to assembly class A, B or C based on plots shown in Fig. 2. Primary peptide data for these experiments and the P4C10 experiments are in the Excel spreadsheet version of Table S1.

	P4					P4C10				P4C10/P4	Stability	Class
Protein	pept	Mean	Std Error	Median	Protein	Pept	Mean	Std Error	Median	obs		
ACO2	120	0.1673	0.0042	0.1580	ACO2	282	0.1180	0.0030	0.1050	0.7050	0.9400	STD
CPS1	1055	0.2337	0.0017	0.2253	CPS1	2717	0.1568	0.0011	0.1433	0.6713	0.8950	STD
CS	161	0.1490	0.0035	0.1367	CS	753	0.1155	0.0019	0.0996	0.7748	1.0331	STD
HADHA	723	0.2219	0.0018	0.2163	HADHA	1117	0.1406	0.0016	0.1276	0.6336	0.8448	STD
HADHB	240	0.1563	0.0033	0.1494	HADHB	480	0.1291	0.0027	0.1121	0.8257	1.1010	STD
HSPA9	608	0.1559	0.0019	0.1453	HSPA9	1617	0.1137	0.0012	0.0984	0.7293	0.9724	STD
HSPD1	2367	0.1296	0.0011	0.1164	HSPD1	8850	0.1024	0.0006	0.0829	0.7899	1.0532	STD
LRPPRC	589	0.1746	0.0022	0.1637	LRPPRC	1746	0.1341	0.0015	0.1180	0.7678	1.0238	STD
MDH2	344	0.1710	0.0030	0.1530	MDH2	1049	0.1161	0.0013	0.1026	0.6788	0.9051	STD
OXCT1	186	0.1615	0.0031	0.1548	OXCT1	534	0.1297	0.0026	0.1140	0.8032	1.0709	STD
PC	257	0.2703	0.0046	0.2647	PC	848	0.1785	0.0023	0.1641	0.6603	0.8803	STD
PHB	331	0.1446	0.0026	0.1346	PHB	779	0.1185	0.0022	0.0994	0.8193	1.0924	STD
PHB2	400	0.1384	0.0024	0.1247	PHB2	1205	0.1070	0.0016	0.0893	0.7735	1.0313	STD
SHMT2	267	0.1805	0.0036	0.1619	SHMT2	1030	0.1359	0.0020	0.1182	0.7525	1.0033	STD
SLC25A5	228	0.1647	0.0035	0.1517	SLC25A5	1345	0.1269	0.0015	0.1124	0.7707	1.0276	STD
SLC25A6	306	0.1934	0.0030	0.1847	SLC25A6	867	0.1476	0.0022	0.1297	0.7629	1.0171	STD
TRAP1	207	0.1698	0.0041	0.1534	TRAP1	623	0.1229	0.0022	0.1039	0.7240	0.9654	STD
TUFM	401	0.1538	0.0028	0.1419	TUFM	1095	0.1133	0.0016	0.0982	0.7368	0.9823	STD
VDAC1	382	0.1382	0.0022	0.1289	VDAC1	940	0.1019	0.0016	0.0870	0.7370	0.9827	STD
	avg=	0.1723				avg=	0.1268			0.7430	0.9906	
	sd=	0.0356				sd=	0.0193			0.0540	0.0720	
Protein	Pept	Mean	Std Error	Median	Protein	Pept	Mean	Std Error	Median	P4C10/P4	Stability	Class
bS1m	64	0.2281	0.0097	0.2108	bS1m	148	0.1423	0.0055	0.1232	0.6239	0.8319	early
uS2m	71	0.3115	0.0130	0.3137	uS2m	105	0.1327	0.0066	0.1129	0.4262	0.5683	early
uS3m	28	0.5681	0.0163	0.5689	uS3m	34	0.0762	0.0079	0.0556	0.1342	0.1789	late
uS5m	63	0.2530	0.0075	0.2510	uS5m	121	0.1357	0.0051	0.1194	0.5365	0.7153	early
bS6m	50	0.2234	0.0111	0.2094	bS6m	127	0.0818	0.0039	0.0686	0.3661	0.4882	
uS7m	131	0.2996	0.0071	0.2928	uS7m	229	0.1183	0.0038	0.1044	0.3949	0.5265	early
uS9m	145	0.1880	0.0047	0.1750	uS9m	225	0.1504	0.0050	0.1322	0.7997	1.0663	early
uS10m	8	0.3707	0.0219	0.3919	uS10m	33	0.1282	0.0126	0.1015	0.3460	0.4613	late
uS11m	13	0.3179	0.0477	0.3236	uS11m	41	0.1004	0.0076	0.0840	0.3158	0.4211	early
uS12m	20	0.2545	0.0085	0.2576	uS12m	28	0.0787	0.0072	0.0600	0.3093	0.4124	early
uS14m	15	0.3010	0.0161	0.2865	uS14m	32	0.1208	0.0101	0.1032	0.4014	0.5352	late
uS15m	9	0.4342	0.0348	0.4218	uS15m	32	0.1775	0.0198	0.1651	0.4087	0.5450	late
bS16m	25	0.2150	0.0093	0.2113	bS16m	10	0.1480	0.0275	0.1098	0.6883	0.9178	early
uS17m	19	0.2434	0.0238	0.2043	uS17m	10	0.1779	0.0294	0.1311	0.7306	0.9742	early
bS18m	21	0.2871	0.0103	0.2863	bS18m	18	0.1230	0.0161	0.1050	0.4283	0.5710	
bS21m	6	0.3793	0.0285	0.3910	bS21m	17	0.1475	0.0213	0.1037	0.3889	0.5186	late
mS22	103	0.2077	0.0098	0.1789	mS22	186	0.1146	0.0044	0.0927	0.5519	0.7359	early
mS23	89	0.2981	0.0082	0.2888	mS23	116	0.1180	0.0064	0.1002	0.3959	0.5279	early
mS25	42	0.2210	0.0122	0.1939	mS25	88	0.1185	0.0070	0.0948	0.5363	0.7151	late
mS26	46	0.2054	0.0126	0.1850	mS26	70	0.1416	0.0094	0.1295	0.6895	0.9193	late
mS27	154	0.2991	0.0053	0.2909	mS27	232	0.1264	0.0037	0.1075	0.4224	0.5632	early
mS29	254	0.3341	0.0049	0.3231	mS29	292	0.1486	0.0043	0.1248	0.4448	0.5931	early
mS31	23	0.1576	0.0150	0.1504	mS31	58	0.1267	0.0090	0.1037	0.8039	1.0719	early
mS33	7	0.1429	0.0078	0.1332	mS33	13	0.1329	0.0197	0.1008	0.9297	1.2396	late
mS34	58	0.2290	0.0081	0.2200	mS34	78	0.1173	0.0064	0.1051	0.5122	0.6830	early
mS35	48	0.4572	0.0150	0.4723	mS35	24	0.0925	0.0093	0.0844	0.2022	0.2696	early
mS37	4	0.5010	0.0280	0.5016	mS37	2	0.0888	0.0367	0.0888	0.1773	0.2364	
mS38	5	0.5887	0.0520	0.6387	mS38	3	0.1384	0.0756	0.0944	0.2350	0.3134	
mS39	130	0.2278	0.0072	0.2068	mS39	148	0.1215	0.0041	0.1088	0.5336	0.7115	early
mS40	89	0.2859	0.0075	0.2842	mS40	92	0.1092	0.0052	0.0937	0.3820	0.5094	early
	avg=	0.3010				avg=	0.1245					
	sd=	0.1128				sd=	0.0254					

Table S2

Protein	Pept	Mean	Std Error	Median		Protein	Pept	Mean	Std Error	Median	P4C10/P4	Stability	Class
uL1m	24	0.1446	0.0056	0.1436		uL1m	62	0.1137	0.0077	0.0983	0.7866	1.0488	int
uL2m	25	0.2346	0.0159	0.2288		uL2m	67	0.1238	0.0075	0.1071	0.5277	0.7036	late
uL3m	53	0.4284	0.0167	0.4441		uL3m	98	0.1163	0.0067	0.1005	0.2716	0.3621	early
uL4m	98	0.3556	0.0104	0.3453		uL4m	124	0.1168	0.0051	0.1044	0.3285	0.4380	early
bL9m	43	0.3226	0.0172	0.3238		bL9m	90	0.1065	0.0047	0.0918	0.3301	0.4402	int
uL10m	27	0.2626	0.0127	0.2493		uL10m	49	0.1729	0.0149	0.1448	0.6582	0.8776	early
uL11m	59	0.3410	0.0133	0.3491		uL11m	107	0.1147	0.0054	0.0967	0.3363	0.4484	int
bL12m	52	0.1598	0.0077	0.1609		bL12m	80	0.0943	0.0042	0.0829	0.5905	0.7873	early
uL13m	81	0.3451	0.0127	0.3535		uL13m	158	0.1277	0.0050	0.1050	0.3701	0.4935	int
uL14m	25	0.3592	0.0193	0.3372		uL14m	65	0.1081	0.0062	0.0935	0.3010	0.4013	early
uL15m	119	0.3062	0.0086	0.3096		uL15m	235	0.1141	0.0038	0.0978	0.3727	0.4969	early
uL16m	27	0.3230	0.0215	0.3193		uL16m	58	0.1136	0.0076	0.0936	0.3518	0.4690	late
bL17m	71	0.4079	0.0216	0.4502		bL17m	186	0.1679	0.0071	0.1431	0.4116	0.5489	early
uL18m	43	0.3887	0.0156	0.3867		uL18m	98	0.1180	0.0041	0.1062	0.3036	0.4049	int
bL19m	107	0.3551	0.0101	0.3802		bL19m	101	0.1192	0.0070	0.0935	0.3356	0.4475	early
bL20m	27	0.3363	0.0176	0.3345		bL20m	52	0.1004	0.0044	0.0971	0.2985	0.3980	early
bL21m	41	0.3294	0.0089	0.3328		bL21m	103	0.1025	0.0049	0.0875	0.3112	0.4150	early
uL22m	58	0.4186	0.0141	0.4025		uL22m	126	0.1170	0.0054	0.0987	0.2794	0.3726	early
uL23m	20	0.1944	0.0106	0.1948		uL23m	32	0.1153	0.0079	0.1082	0.5929	0.7906	late
uL24m	32	0.2494	0.0118	0.2541		uL24m	77	0.1467	0.0089	0.1178	0.5883	0.7844	late
bL27m	45	0.4052	0.0109	0.3859		bL27m	94	0.1002	0.0038	0.0915	0.2472	0.3296	int
bL28m	46	0.2601	0.0090	0.2436		bL28m	55	0.1100	0.0078	0.0915	0.4229	0.5639	late
uL29m	54	0.3982	0.0206	0.4065		uL29m	136	0.1414	0.0076	0.1091	0.3552	0.4736	int
uL30m	26	0.3424	0.0202	0.3652		uL30m	58	0.0948	0.0066	0.0793	0.2769	0.3691	int
bL31m	4	0.1942	0.0057	0.1916		bL31m	16	0.1518	0.0230	0.1142	0.7816	1.0421	late
bL32m	5	0.2707	0.0230	0.2368		bL32m	11	0.0884	0.0166	0.0640	0.3264	0.4352	early
bL33m	5	0.4375	0.0663	0.3569		bL33m	12	0.1457	0.0210	0.1168	0.3330	0.4441	late
bL34m	18	0.2798	0.0217	0.2682		bL34m	30	0.1063	0.0105	0.0874	0.3799	0.5066	int
bL35m	5	0.2797	0.0258	0.2459		bL35m	14	0.1942	0.0337	0.2067	0.6946	0.9261	late
mL37	70	0.3412	0.0122	0.3315		mL37	133	0.1372	0.0062	0.1155	0.4021	0.5362	late
mL38	81	0.3448	0.0149	0.3591		mL38	122	0.1408	0.0062	0.1230	0.4083	0.5444	early
mL39	79	0.2993	0.0099	0.2975		mL39	178	0.1297	0.0046	0.1074	0.4334	0.5778	early
mL40	20	0.2213	0.0122	0.2144		mL40	55	0.1149	0.0073	0.1028	0.5190	0.6921	early
mL41	25	0.2279	0.0152	0.2131		mL41	32	0.1495	0.0119	0.1284	0.6561	0.8748	late
mL42	8	0.3180	0.0238	0.3036		mL42	34	0.0960	0.0087	0.0812	0.3020	0.4026	early
mL43	41	0.2414	0.0134	0.2453		mL43	58	0.1241	0.0092	0.1018	0.5141	0.6854	early
mL44	73	0.2907	0.0098	0.2771		mL44	143	0.1441	0.0066	0.1268	0.4958	0.6611	early
mL45	62	0.3305	0.0114	0.3229		mL45	76	0.1196	0.0066	0.0987	0.3618	0.4823	early
mL46	6	0.1996	0.0762	0.1269		mL46	53	0.1382	0.0098	0.1189	0.6922	0.9229	early
mL48	15	0.2454	0.0140	0.2382		mL48	45	0.1178	0.0087	0.0903	0.4799	0.6399	early
mL49	35	0.3156	0.0199	0.2925		mL49	80	0.1217	0.0075	0.0999	0.3857	0.5143	early
mL50	53	0.2799	0.0127	0.2733		mL50	136	0.1274	0.0056	0.1053	0.4551	0.6068	early
mL51	4	0.5263	0.0816	0.5205		mL51	11	0.1645	0.0196	0.1536	0.3125	0.4167	int
mL52	12	0.5282	0.0329	0.5000		mL52	12	0.2903	0.0730	0.2837	0.5495	0.7327	
mL53	24	0.3740	0.0218	0.3463		mL53	64	0.1885	0.0110	0.1739	0.5039	0.6719	int
mL54	3	0.1538	0.0070	0.1552		mL54	15	0.1350	0.0178	0.1175	0.8778	1.1704	late
mL62	16	0.2657	0.0120	0.2580		mL62	68	0.1180	0.0060	0.1068	0.4442	0.5923	int
mL63	13	0.3757	0.0767	0.4561		mL63	20	0.1993	0.0204	0.2001	0.5304	0.7072	early
mL64	32	0.5950	0.0329	0.6490		mL64	41	0.1629	0.0143	0.1365	0.2738	0.3651	late
mL65	36	0.4497	0.0252	0.4207		mL65	47	0.1305	0.0143	0.0969	0.2902	0.3870	late
mL66	48	0.2407	0.0110	0.2410		mL66	81	0.1288	0.0068	0.1079	0.5351	0.7135	int
	avg=	0.3195					avg=	0.1318					
	sd=	0.09486					sd=	0.0341					

Table S2. MRPs are imported into mitochondria in excess and can be unstable if not assembled, related to Figure 4. Summary of H:L ratio data for MRPs and selected abundant standard proteins observed by LC-MS/MS SCX-C18 (mudpit) analysis of tryptic digests of whole mitochondrial fractions following 4 hr pulse SILAC labeling with and without a 10 hr chase. The P4C10/P4 ratio is shown to indicate the change in mean H:L ratio during the chase. The stability parameter compares the P4C10/P4 ratio to the value of 0.75 expected for a 10 hr chase based on exponential growth of cells with a generation time of 24 hr.

Table S2, cont.

Protein	3 Hr Mean	4 Hr Mean	6 Hr Mean	12 Hr Mean	P4C10/P4	Class
uL15m	0.0359	0.0607	0.1065	0.3208	1.758	early
uL4m	0.0359	0.0577	0.1214	0.3215	2.019	early
mL49	0.0371	0.0590	0.1144	0.3475	1.938	early
mL50	0.0334	0.0474	0.0822	0.2831	2.112	early
uL3m	0.0492	0.0743	0.1080	0.3341	1.473	early
bL19m	0.0447	0.0530	0.1015	0.3251	2.081	early
uL14m	0.0456	0.0690	0.1317	0.3902	1.596	early
bL17m	0.0372	0.0678	0.1253	0.3611	1.604	early
uL22m	0.0459	0.0699	0.1055	0.3496	1.533	early
bL32m	0.0486	0.0713	0.1086	0.3509	1.461	early
mL39	0.0352	0.0561	0.0907	0.2829	1.993	early
mL45	0.0507	0.0733	0.1104	0.3346	1.471	early
bL20m	0.0395	0.0390	0.1036	0.3152	2.782	early
bL21m	0.0345	0.0605	0.1027	0.3276	1.843	early
mL42	0.0260	0.0392	0.0929	0.3213	2.611	early
mL43	0.0416	0.0649	0.1047	0.3125	1.709	early
mL44	0.0362	0.0557	0.1008	0.3091	2.001	early
mL40	0.0535	0.0633	0.1242	0.3599	1.746	early
mL46	0.0385	0.0679	0.1055	0.2909	1.256	early
mL48	0.0556	0.0711	0.1356	0.3661	1.475	early
uL10m	0.0486	0.0575	0.1097	0.2855	1.825	early
bL12m	0.0289	0.0404	0.0876	0.2295	2.323	early
mL38	0.0411	0.0628	0.1166	0.3279	1.878	int
mL62	0.0531	0.0926	0.1514	0.3931	1.168	int
uL18m	0.0596	0.0880	0.1414	0.3851	1.286	int
bL27m	0.0570	0.0961	0.1465	0.4072	1.200	int
uL1m	0.0552	0.0895	0.1557	0.3663	1.016	int
mL51	0.0651	0.0730	0.1518	0.4005	1.822	int
mL53	0.0610	0.0824	0.1345	0.3630	1.211	int
uL11m	0.0655	0.0893	0.1551	0.3876	1.178	int
uL13m	0.0615	0.0908	0.1595	0.4110	1.290	int
mL66	0.0598	0.0864	0.1534	0.3535	1.250	int
uL30m	0.0643	0.0708	0.1265	0.3526	1.492	int
mL63	0.0466	0.0750	0.1244	0.3840	1.554	int
uL29m	0.0550	0.0886	0.1395	0.3963	1.205	int
bL34m	0.0633	0.0774	0.1414	0.3866	1.397	int
mL41	0.0762	0.0978	0.1699	0.4302	1.254	late
uL23m	0.0767	0.1040	0.1597	0.4067	1.105	late
uL24m	0.0725	0.1173	0.1820	0.4352	0.975	late
bL9m	0.0640	0.0909	0.1576	0.4158	1.213	late
bL28m	0.0750	0.1030	0.1819	0.4312	1.130	late
mL65	0.0801	0.1076	0.1827	0.4615	1.106	late
mL37	0.0755	0.0975	0.1777	0.4639	1.149	late
uL2m	0.1020	0.1234	0.1990	0.4695	0.926	late
uL16m	0.1079	0.1324	0.2149	0.4994	0.942	late
mL54	0.0810	0.0907	0.1520	0.3463	1.152	late
bL31m	0.0718	0.1097	0.1771	0.4803	1.054	late
mL64	0.0801	0.1006	0.1790	0.4431	1.185	late
bL35m	0.0920	0.1243	0.2141	0.4905	0.777	late
bL33m	0.2097	0.2899	0.4782	1.1153	0.387	late
mL52 and mL36 omitted						

Protein	3 Hr Mean	4 Hr Mean	6 Hr Mean	12 Hr Mean	P4C10/P4	Class
bS16m	0.0322	0.0449	0.0711	0.1367	1.914	early
mS22	0.0423	0.0666	0.1002	0.1593	1.106	early
mS40	0.0405	0.0706	0.0806	0.2174	1.188	early
mS27	0.0432	0.0623	0.0891	0.1749	1.500	early
mS34	0.0316	0.0514	0.0795	0.1519	1.416	early
uS5m	0.0586	0.0674	0.0991	0.2151	1.352	early
uS7m	0.0372	0.0607	0.0856	0.2103	1.148	early
mS29	0.0392	0.0629	0.0838	0.1991	1.640	early
mS31	0.0308	0.0592	0.0726	0.1976	1.512	early
mS35	0.0451	0.0581	0.1065	0.3199	1.523	early
uS9m	0.0506	0.0749	0.0721	0.1612	0.868	early
mS39	0.0553	0.0653	0.0912	0.2377	1.407	early
uS11m	0.0330	0.0410	0.1144	0.2801	2.366	early
uS12m	0.0517	0.0698	0.1203	0.2795	1.254	early
uS17m	0.0376	0.0404	0.0523	0.1588	1.778	early
mS23	0.0436	0.0701	0.0830	0.2035	1.005	early
uS2m	0.0492	0.0801	0.0933	0.2373	1.207	early
bS1m	0.0486	0.0695	0.1050	0.1490	1.085	early
uS3m	0.0893	0.1399	0.2182	0.4301	0.653	late
mS33	0.0703	0.1077	0.1892	0.4042	0.855	late
uS10m	0.0422	0.0978	0.1267	0.3013	1.045	late
uS14m	0.1184	0.1697	0.2358	0.5215	0.667	late
uS15m	0.0812	0.1018	0.1568	0.3341	1.006	late
mS25	0.0494	0.1240	0.0732	0.1881	0.572	late
mS26	0.0512	0.1093	0.1204	0.1549	0.813	late
bS21m	0.0996	0.1262	0.1833	0.4744	0.891	late

bS6m, bS18m, mS37, mS38 omitted

Table S3. MRP order of assembly, related to Figures 5, 6 and 7. Data on the full pattern for ribosome H:L ratios derived from Table S1 were combined with the pulse-chase timing data (P4/P4C10) related to Figure 3. Boxes and differential coloring are used to highlight modular clusters of proteins that bind at similar stages and share extensive binding interfaces (Figure S4, generally >1000 $Å^2$). The MRPs were assigned to early, intermediate (int) or late assembly cohorts as discussed in the text.

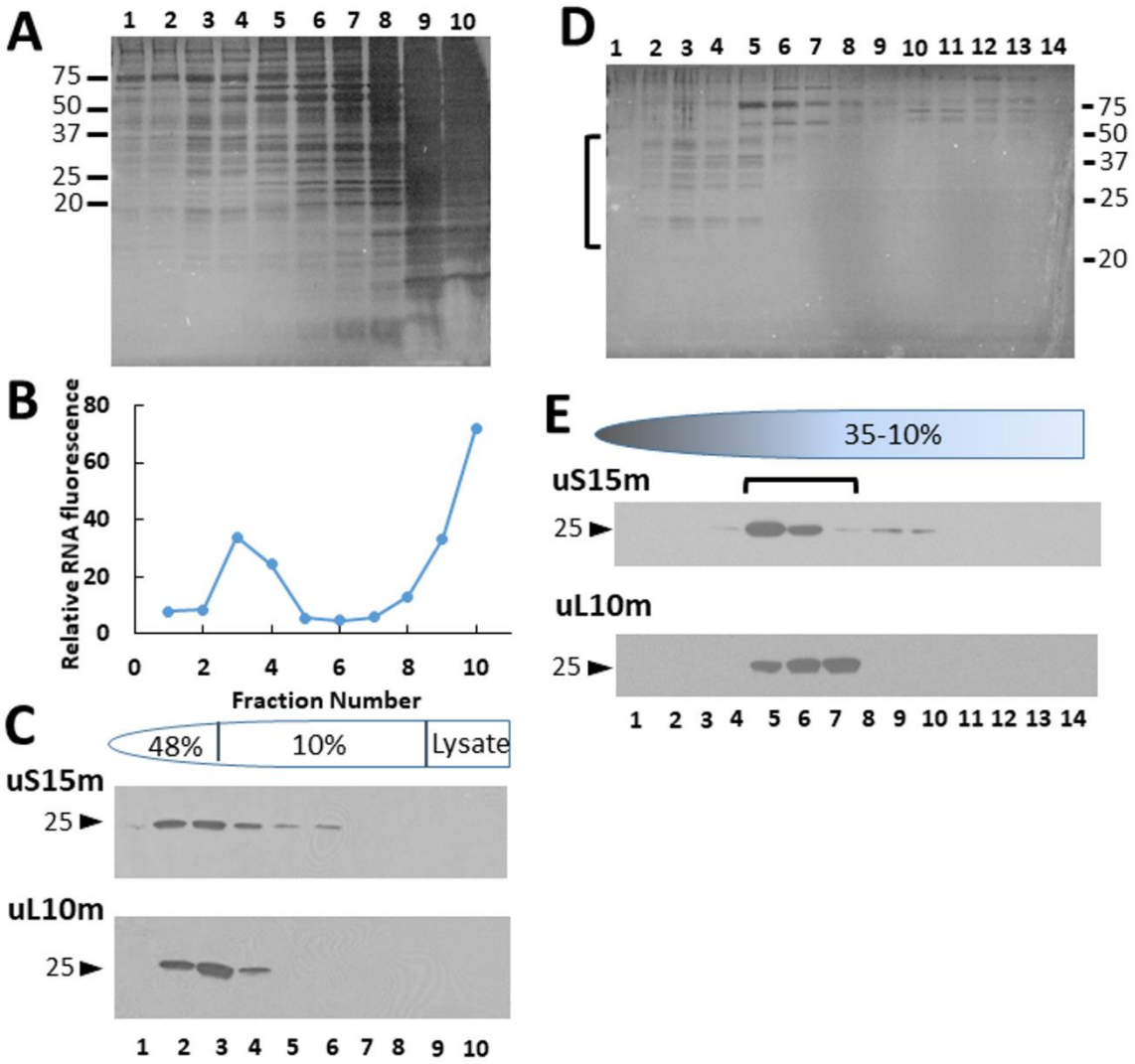

Figure S1. Preparation of SILAC labeled mitoribosomes, related to Experimental Procedures.

A. Mitoribosomes were prepared from mitochondrial lysates using two successive high salt sucrose gradients. The short-term spin was used to separate mitoribosomes from the great majority of non-ribosomal proteins as shown by a silver-stained gel of gradient fractions. The sizes of mobility markers in kDa are shown on the left.

B. Fractions were collected from the bottom of the tube and a 7 µl sample of each fraction was taken for RNA staining using SybrGreen II assayed in a microtiter well format. Rapidly sedimenting fractions with the peak of RNA fluorescence were combined, concentrated by ultrafiltration and loaded on the second gradient.

C. Samples of each fraction from the short-term spin were reserved for later analysis by SDS-PAGE and immunoblotting with antibodies to confirm the location of mitoribosomes. Immunoblots for LSU (uL10m) and SSU (uS15m) in gel regions near the 25 kDa mobility marker.

D. The second sucrose gradient was also fractionated from the tube bottom. An example of a silver stained gel of one preparation is shown. In this instance the cluster of rapidly sedimenting low molecular mass proteins in fractions 2-5 (vertical bracket) is characteristic of MRPs. The sizes of mobility markers in kDa are shown on the right.

E. In routine preparations, samples were analyzed by SDS-PAGE and immunoblotting was used to identify fractions containing mitoribosome markers. In this example, proteins in fractions 5-7 indicated by the horizontal bracket were precipitated and submitted for mass spectrometry. Note that silver staining of gels was not done routinely and the samples shown in A and D are from different preparations than the other illustrations. Labels on the side of silver stained gels show the positions of pre-stained markers, in kDa. The arrowheads in the immunoblots in C and E indicate the position of the 25 kDa mobility marker on SDS-PAGE.

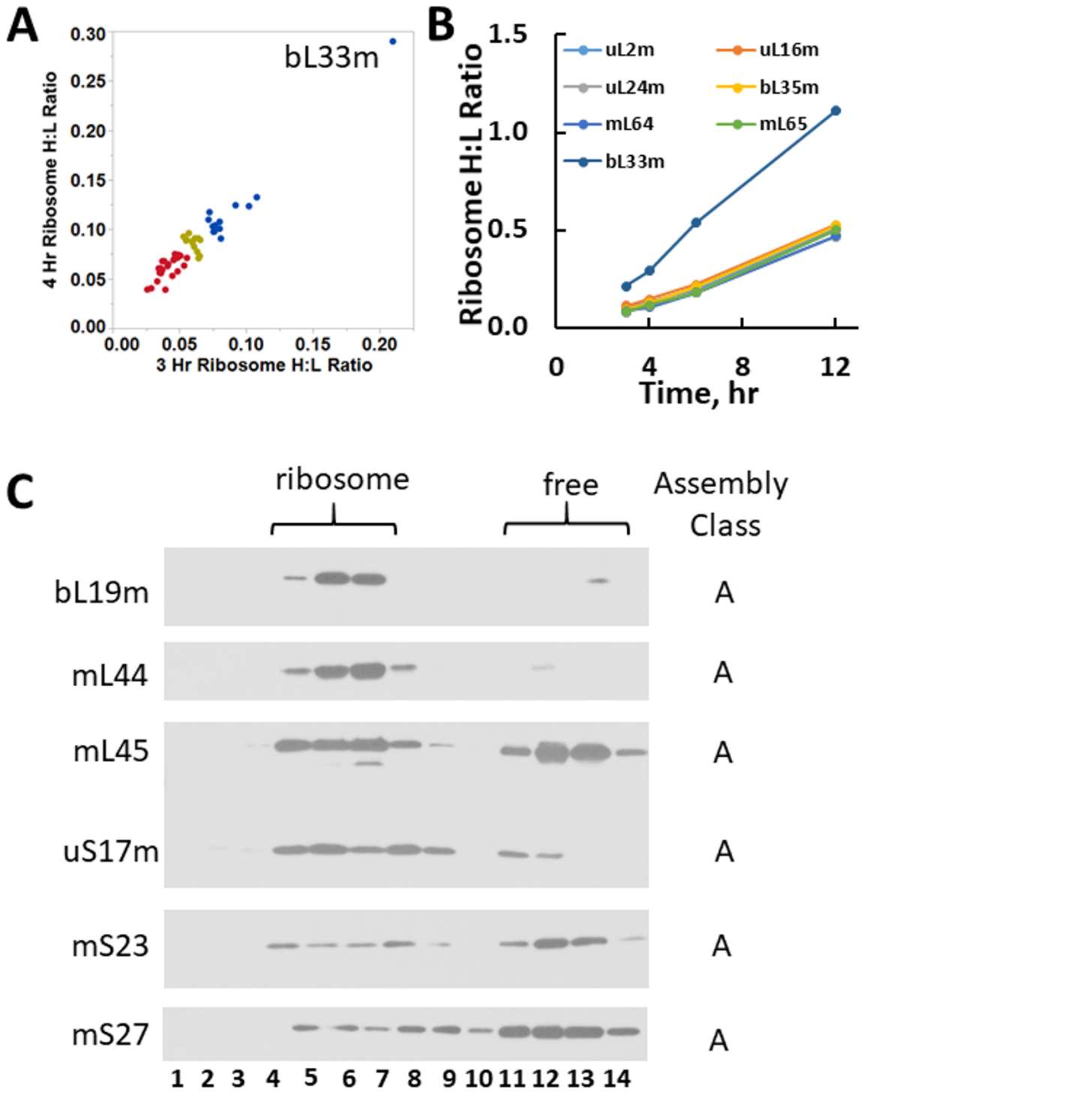

Figure S2. Testing alternative hypotheses to explain variation in rates of appearance of nascent MRPs in mitoribosomes, related to Figure 2.

A. bL33m is incorporated into mitoribosomes at a much faster rate than other late MRPs. The chart shows the H:L ratio of LSU MRPs including bL33m in purified mitoribosomes after 3 hr (abscissa) and 4 hr (ordinate) of SILAC labeling.

B. The H:L ratio of bL33m in mitoribosomes continues to increase with increasing SILAC labeling time at a rate greater than that of other late-binding LSU proteins which generally accumulate at the rate expected for the additional synthesis of new mitoribosomes in exponentially growing cells as shown in Fig. 2. bL33m clearly behaves as an outlier and exemplifies the behavior of an MRP that readily dissociates from mitoribosomes and is replaced with newly-synthesized protein.

C. Western blots of sucrose gradient fractions showing that MRPs that appear slowly in mitoribosomes (Class A) vary in the relative amount of free and ribosome-bound proteins.

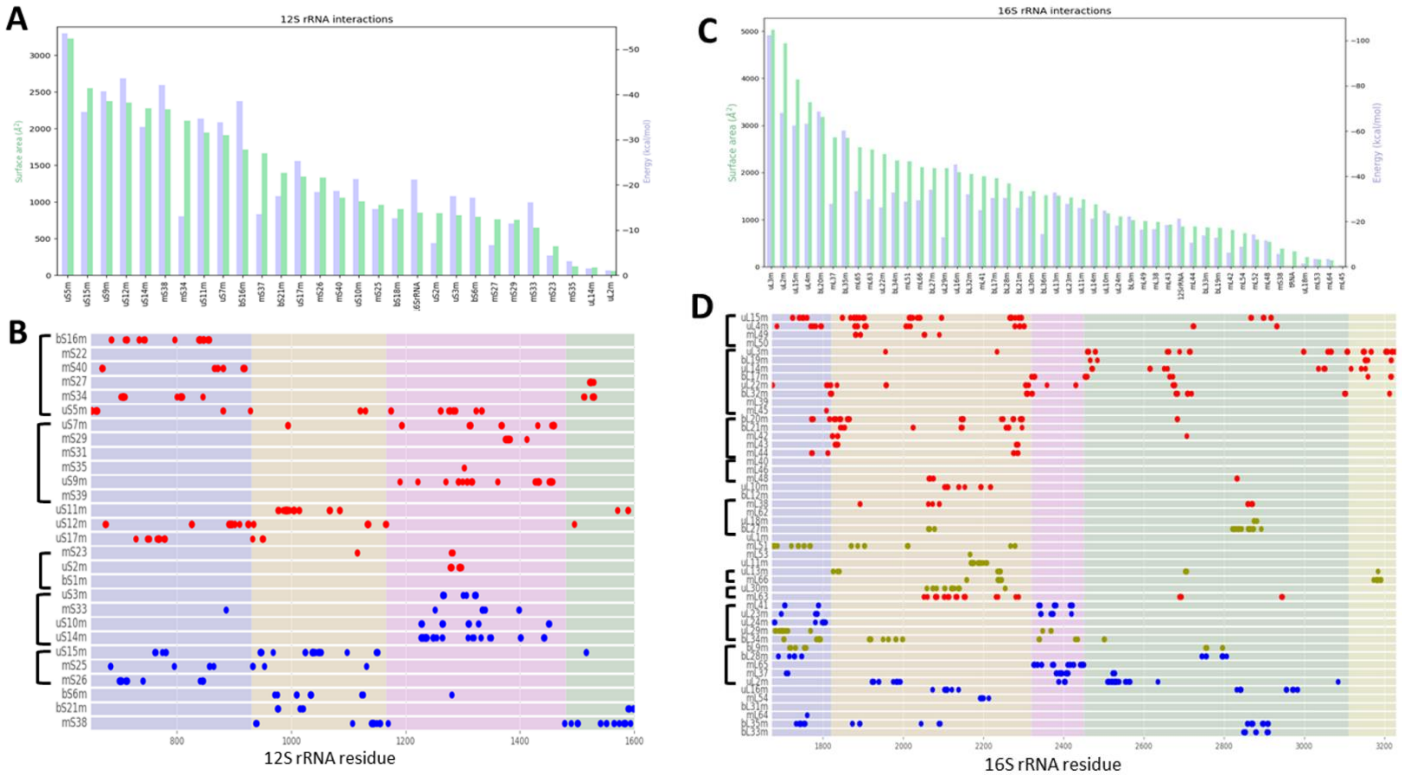

Figure S3. RNA binding analyses, related to Figures 5 and 6.

A, C. The cryoEM model 3J9M was analyzed to derive the RNA-protein buried surface area (green) and estimated binding energy (blue) for interaction of the indicated proteins with the 12S rRNA (A) and the 16S rRNA (C) using PDBePISA.

B, D. Locations of contact regions between individual proteins and RNAs with sufficient proximity and H-bond interaction potential are shown for the SSU (B) and LSU (D). The differently colored regions of the RNA correspond to conventional structural domains. Dots indicating contact sites are colored according to the Early (red), Intermediate (pea green) or Late (blue) assembly class of the protein. Brackets shown indicate sets of proteins that share similar assembly kinetics (Table S3) and extensive protein-protein interaction surfaces (Figure S4).

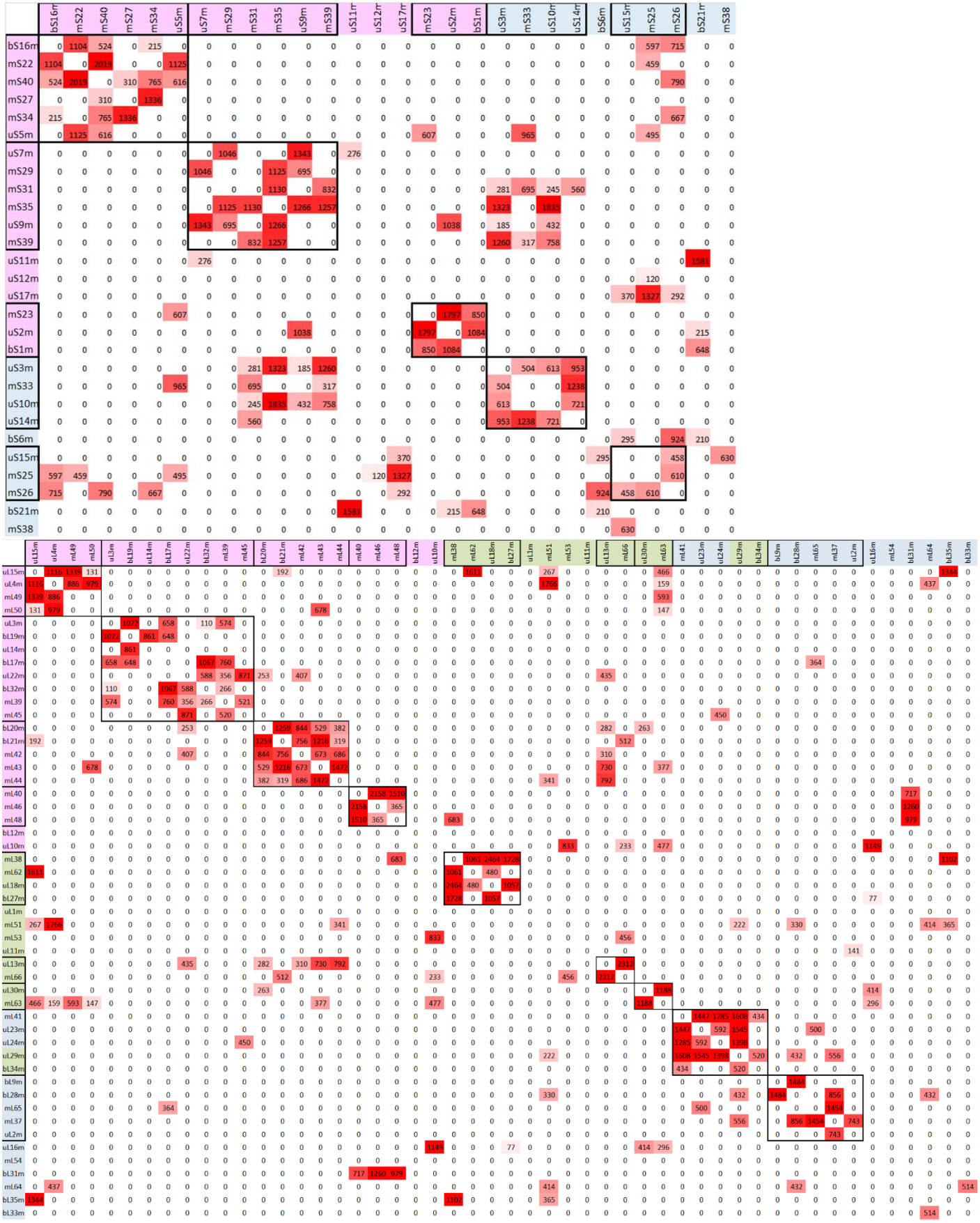

Figure S4. Two-dimensional display of the protein-protein interactions surface areas for SSU (Top) and LSU (Bottom), related to Figures 5, 6 and 7. Interactions were determined using the PDBePISA site (www.ebi.ac.uk/pdbe/pisa/) and proteins were grouped according to their assembly kinetics as in Table S3 with subgroups based on high mutual interaction surface area surrounded by heavy borders. The numbers indicate BSA in Å^2 and the red color intensity increases as the BSA approaches or exceeds 1000 Å^2.

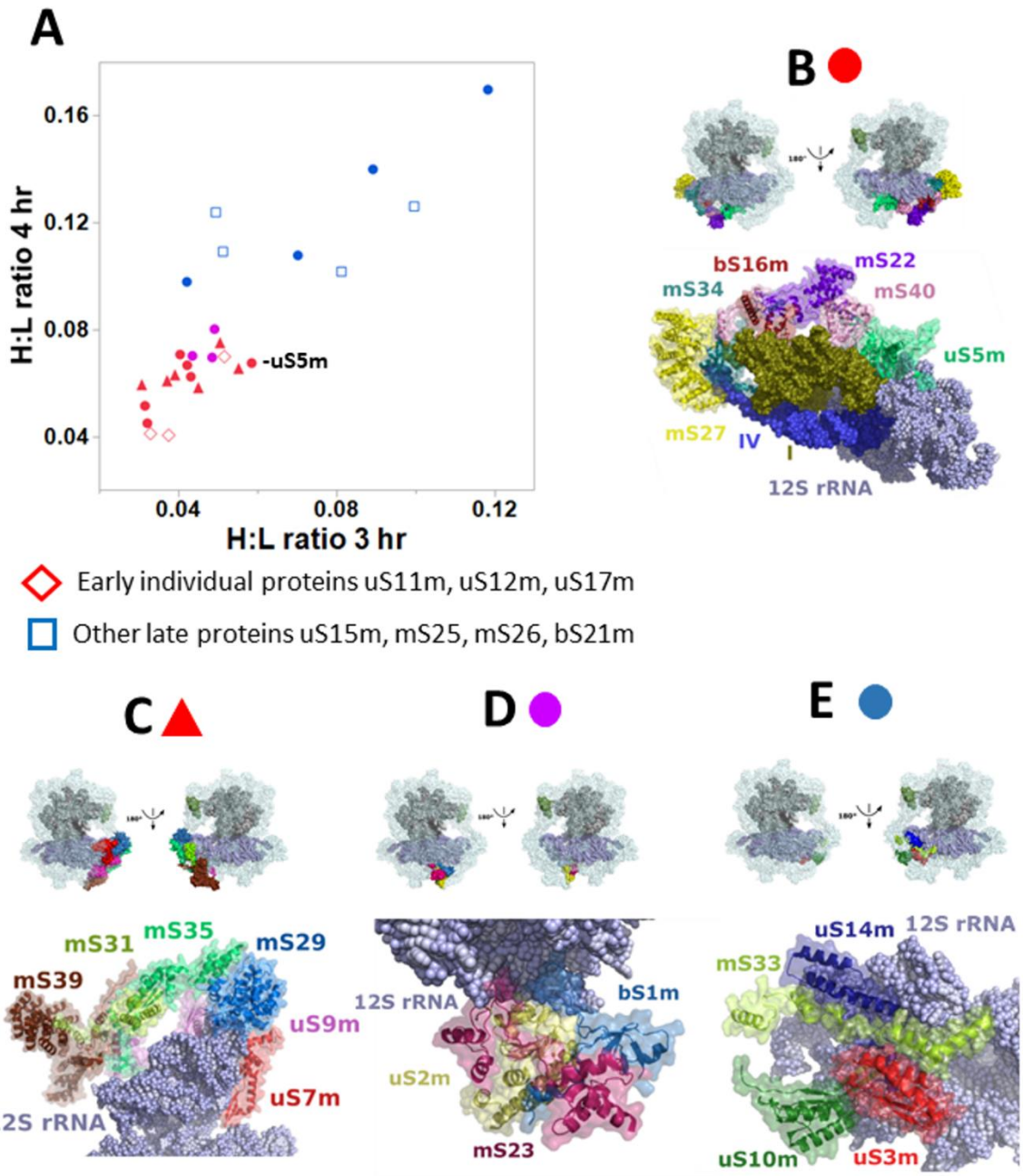

Figure S5. Sets of SSU MRPs share extensive contacts and similar assembly kinetics, related to Figure 5. For each set, the larger structure shows an expanded view of the group members with distinct coloration, unrelated to binding kinetics, as well as a pair of images to show the location of the group in the overall mitoribosome structure from two points of view. The MRPs not under consideration in each figure are shown as light colored surface contours surrounding the rRNA core. The scatterplots illustrate the similar kinetic behavior of group members. Recall that H:L values have a statistical error not reflected in the figure, generally approximately +/-10% of the mean value. Therefore, a general clustering of points is considered significant.

A. Graph showing the H:L values of SSU proteins after 3 hr and 4hr of labeling as in Figure 2 except that sets of proteins sharing extensive BSA are identified by distinct symbols identified in panels B-E. The H:L values for some additional early- and late-binding proteins that do not share extensive BSA with other proteins are also shown as open red diamonds or open blue square data points.

B. bS16m and mS40 bind to Domain I of 12S rRNA (gold spheres) along with mS22, which does not contact the rRNA directly. Strong interactions of these proteins with mS34 and mS27 bring the 3' Domain IV of 12S rRNA (blue spheres) into juxtaposition with Domain I. uS5m binds slightly later to this group. The scatterplot also shows the binding kinetics of uS11m and uS17m, which do not show tight interactions with other early-binding MRPs.

C. uS7m, mS29 and uS9m make contacts with the head region of 12S rRNA, recruiting mS35, mS31 and mS39, all of which have minimal or no contact with RNA.

D. bS1m, uS2m and mS23 form a compact trimer that binds to the outer surface of 12S RNA, away from the intersubunit interface.

E. uS3m, uS10m, mS33 and uS14m bind to the head region of the SSU with late assembly kinetics that contrast to those of the uS7m group in panel C.

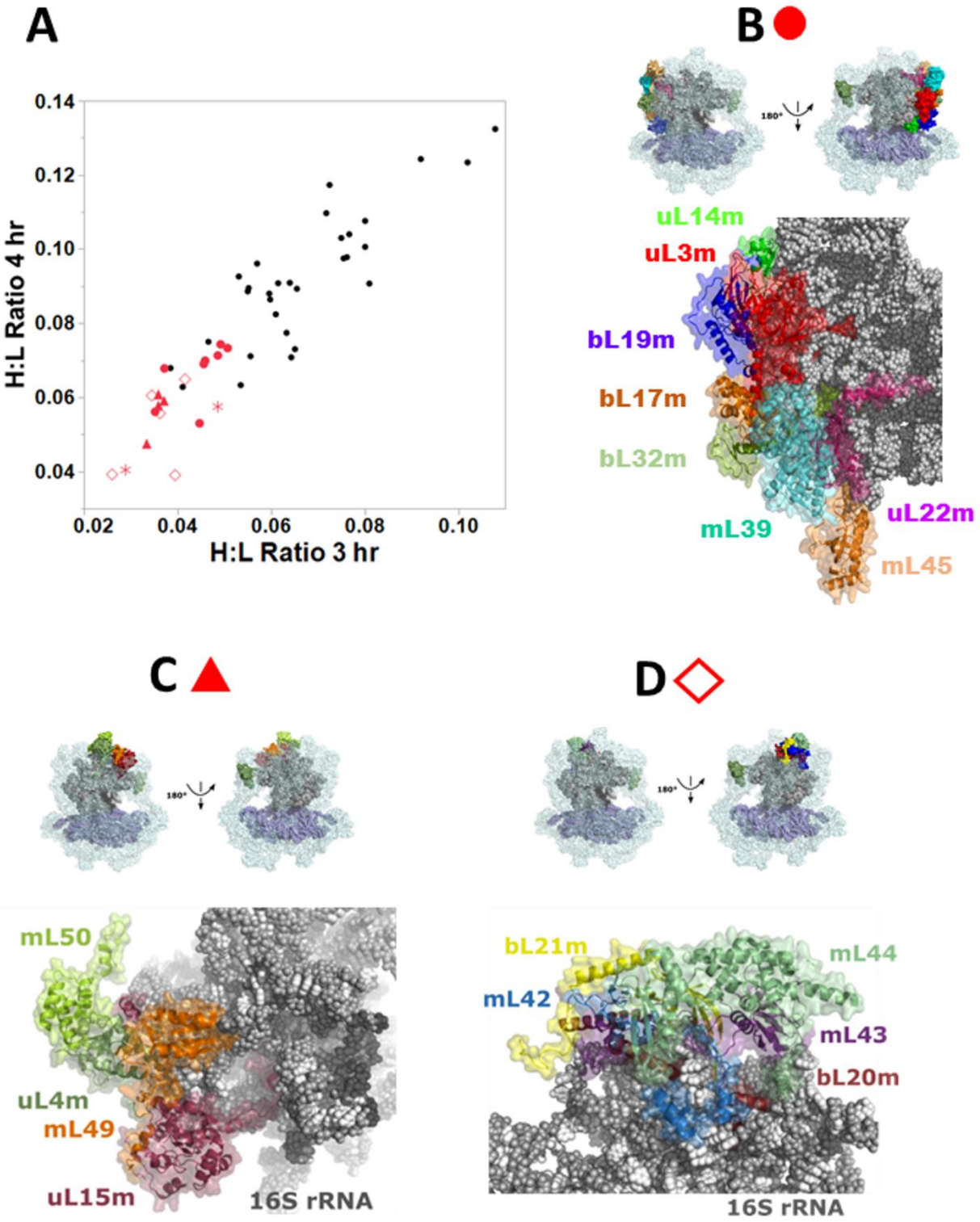

Figure S6. Early-binding LSU proteins assemble in distinct regions as clusters of proteins with extensive BSA and similar assembly kinetics, related to Figures 6 and 7.

A. Scatterplot as in Figure 2B but showing early assembly kinetics of LSU proteins with three sets of mutually-interacting proteins shown with red symbols keyed to panels B-D. The scatterplot also shows with asterisks the binding kinetics of uL10m, which does not show tight interactions with other early-binding MRPs, and bL12m, which is absent from the structural model, but behaves as an early binding protein.

B. uL3m and bL19m extend deeply into 16S rRNA to anchor a group including mL39 and uL22m. Coordinate binding of mL45 dependent on mL39 helps establish one wall of the peptide exit channel. Both mL39 and mL45 lack contacts with rRNA.

C. uL4m-uL15m loop deeply into 16S rRNA and associate with mL49 and mL50, which does not directly contact the RNA.

D. A compact group with extensive contacts to domain 2 of 16S rRNA (bL20m, bL21m, mL42, mL43, mL44) binds with tightly coordinated kinetics.

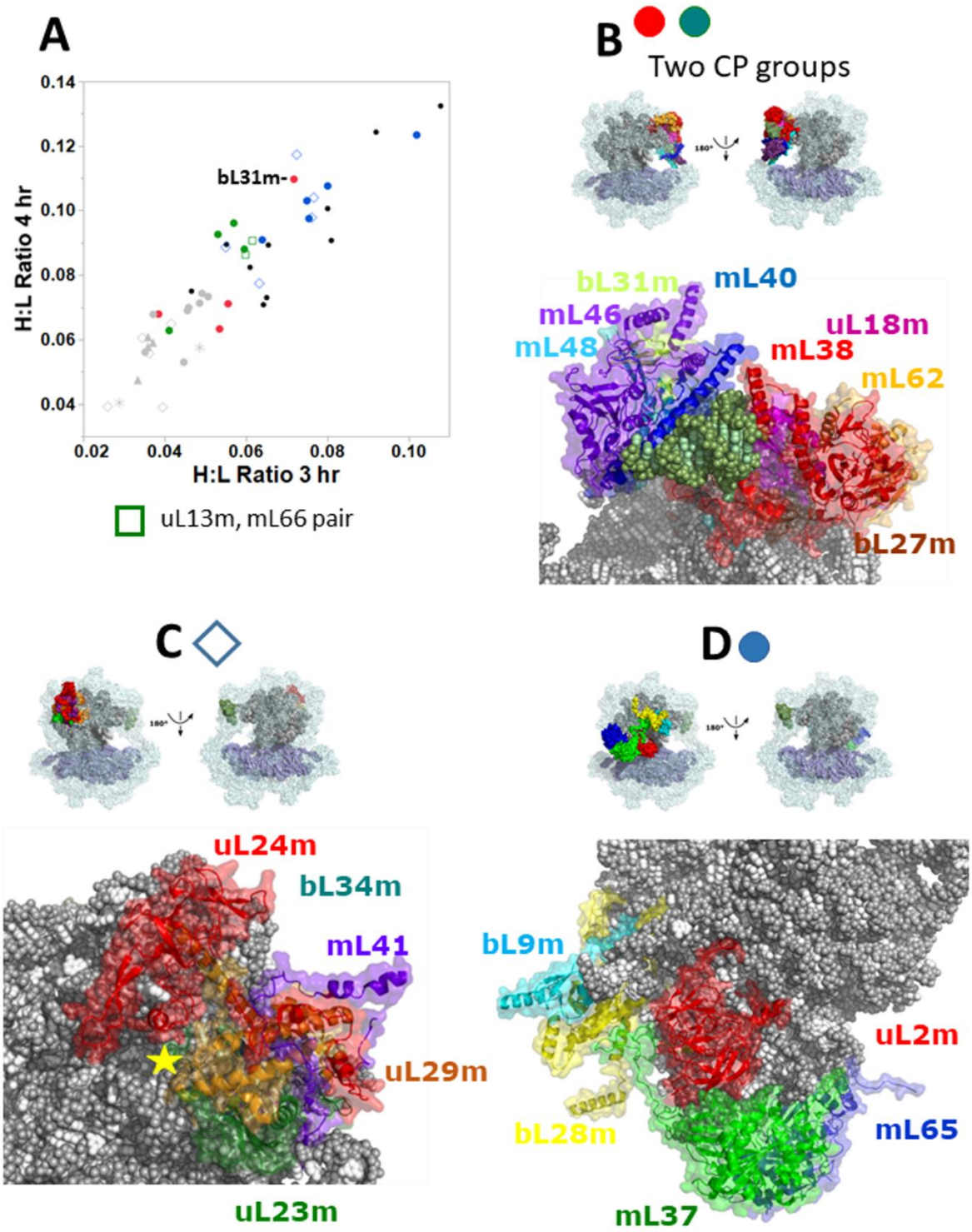

Figure S7. Coordinate binding of proteins with extensive BSA at intermediate and late stages of LSU assembly, related to Figures 6 and 7.

A. Scatterplot as in Figure 2B showing assembly kinetics and locations of two groups of proteins binding near the central protuberance (CP) and of two other groups that join the LSU at later stages in assembly. The binding kinetics of the uL13m-mL66 pair is also shown by open green squares.

B. The central protuberance (CP) of the LSU features $tRNA^{V}$ (green spheres) nested between two groups of interacting proteins. mL40, mL46 and mL48 occupy one face of the tRNA and bind with similar kinetics. bL31m is surrounded by these proteins in the final structure, but exhibits kinetics characteristic of a late-binding protein (Table S1). mL38, uL18m, bL27m and mL62 comprise a second CP group that binds with slightly later kinetics.

C. uL23m, uL24m, uL29m and mL41 bind with intermediate kinetics to form a surface of the peptide exit channel indicted by a star. Binding of this group may involve a major rRNA conformational change to enclose bL34m at a deep location in contact with 16 rRNA.

D. The uL2m-mL37 dimer is the core of a late-binding group with extensions to bL28m, bL9m and mL65.